NASA/TM-1999-209013

Boundary-Layer Transition Results From the F-16XL-2 Supersonic Laminar Flow Control Experiment

Laurie A. Marshall
NASA Dryden Flight Research Center
Edwards, California

December 1999

The NASA STI Program Office...in Profile

Since its founding, NASA has been dedicated to the advancement of aeronautics and space science. The NASA Scientific and Technical Information (STI) Program Office plays a key part in helping NASA maintain this important role.

The NASA STI Program Office is operated by Langley Research Center, the lead center for NASA's scientific and technical information. The NASA STI Program Office provides access to the NASA STI Database, the largest collection of aeronautical and space science STI in the world. The Program Office is also NASA's institutional mechanism for disseminating the results of its research and development activities. These results are published by NASA in the NASA STI Report Series, which includes the following report types:

- TECHNICAL PUBLICATION. Reports of completed research or a major significant phase of research that present the results of NASA programs and include extensive data or theoretical analysis. Includes compilations of significant scientific and technical data and information deemed to be of continuing reference value. NASA's counterpart of peer-reviewed formal professional papers but has less stringent limitations on manuscript length and extent of graphic presentations.

- TECHNICAL MEMORANDUM. Scientific and technical findings that are preliminary or of specialized interest, e.g., quick release reports, working papers, and bibliographies that contain minimal annotation. Does not contain extensive analysis.

- CONTRACTOR REPORT. Scientific and technical findings by NASA-sponsored contractors and grantees.

- CONFERENCE PUBLICATION. Collected papers from scientific and technical conferences, symposia, seminars, or other meetings sponsored or cosponsored by NASA.

- SPECIAL PUBLICATION. Scientific, technical, or historical information from NASA programs, projects, and mission, often concerned with subjects having substantial public interest.

- TECHNICAL TRANSLATION. English-language translations of foreign scientific and technical material pertinent to NASA's mission.

Specialized services that complement the STI Program Office's diverse offerings include creating custom thesauri, building customized databases, organizing and publishing research results...even providing videos.

For more information about the NASA STI Program Office, see the following:

- Access the NASA STI Program Home Page at ***http://www.sti.nasa.gov***

- E-mail your question via the Internet to help@sti.nasa.gov

- Fax your question to the NASA Access Help Desk at (301) 621-0134

- Telephone the NASA Access Help Desk at (301) 621-0390

- Write to:
  NASA Access Help Desk
  NASA Center for AeroSpace Information
  7121 Standard Drive
  Hanover, MD 21076-1320

NASA/TM-1999-209013

Boundary-Layer Transition Results From the F-16XL-2 Supersonic Laminar Flow Control Experiment

Laurie A. Marshall
NASA Dryden Flight Research Center
Edwards, California

National Aeronautics and
Space Administration

Dryden Flight Research Center
Edwards, California 93523-0273

December 1999

NOTICE

Use of trade names or names of manufacturers in this document does not constitute an official endorsement of such products or manufacturers, either expressed or implied, by the National Aeronautics and Space Administration.

Available from the following:

NASA Center for AeroSpace Information (CASI)
7121 Standard Drive
Hanover, MD 21076-1320
(301) 621-0390

National Technical Information Service (NTIS)
5285 Port Royal Road
Springfield, VA 22161-2171
(703) 487-4650

CONTENTS

ABSTRACT

A variable-porosity suction glove has been flown on the F-16XL-2 aircraft to demonstrate the feasibility of this technology for the proposed High-Speed Civil Transport (HSCT). Boundary-layer transition data have been obtained on the titanium glove primarily at Mach 2.0 and altitudes of 53,000–55,000 ft. The objectives of this supersonic laminar flow control flight experiment have been to achieve 50- to 60-percent–chord laminar flow on a highly swept wing at supersonic speeds and to provide data to validate codes and suction design. The most successful laminar flow results have not been obtained at the glove design point (Mach 1.9 at an altitude of 50,000 ft). At Mach 2.0 and an altitude of 53,000 ft, which corresponds to a Reynolds number of 22.7×10^6, optimum suction levels have allowed long runs of a minimum of 46-percent–chord laminar flow to be achieved. This paper discusses research variables that directly impact the ability to obtain laminar flow and techniques to correct for these variables.

NOMENCLATURE

A	area of the region, ft^2
BL	butt line, in.
c	chord, in.
C_p	coefficient of pressure, $\frac{p - p_\infty}{\bar{q}_\infty}$
C_q	suction coefficient, $-\frac{m_{flow}}{\rho_\infty U_\infty}$
$C_{q_{MR}}$	multiple-region suction coefficient, $\frac{\sum_{R=i}^{f} C_{q_R} A_R}{\sum_{R=i}^{f} A_R}$
f	final suction region
FCV	flow control valve
FS	fuselage station, in.
H_p	pressure altitude, ft
HSCT	High-Speed Civil Transport
i	initial suction region
L	laminar flow
LSHF	lower-surface hot film
LT	laminar flow with turbulent bursts
M	Mach number
m_{flow}	mass flow for each unit area, $(lbm/sec)/ft^2$

p	pressure, lbf/ft^2
$\bar{q}$	dynamic pressure, lbf/ft^2
R	suction region
Re	Reynolds number
Re/ft	unit Reynolds number, 1/ft
T	turbulent flow
TL	turbulent flow with laminar bursts
TR	peak transition flow
U	velocity, ft/sec
x	chord-wise distance from the leading edge
x/c	chord location (nondimensional)
α	angle of attack, deg
β	angle of sideslip, deg
ρ	density, lbm/ft^3
∞	free-stream condition

INTRODUCTION

Laminar flow control has long been considered as a potentially viable technique for increasing aircraft performance. Previous studies have demonstrated that laminar flow control could reduce takeoff gross weight, mission fuel burn, structural temperatures, emissions, and sonic boom.[1–3] The NASA High-Speed Research program has obtained data to quantify the benefits of this technology.

In response to interest in implementing this technology on the proposed High-Speed Civil Transport (HSCT), NASA initiated the F-16XL Supersonic Laminar Flow Control (SLFC) flight program. This research project used two prototype F-16XL aircraft. The F-16XL-1 project, using active (with suction) and passive (without suction) gloves on the left wing, demonstrated that laminar flow can be achieved on a highly swept–wing configuration at supersonic speeds.[4] Pressure-distribution and transition data were obtained for a Mach range of 1.2–1.7 and an altitude range of 35,000–55,000 ft. The results show that large regions of laminar flow can be achieved when active laminar flow control is used. Flight results also indicate that the attachment line does not have to be located at the leading edge to be laminar.[5]

The first phase of the F-16XL-2 project, using a passive wing glove on the right wing of the aircraft, studied the effects of attachment line, leading-edge radius, and very high Reynolds number on the boundary layer.[4] A primary goal of the passive glove experiment was to obtain detailed surface pressure–distribution data in the leading-edge region. These data were obtained for a Mach range of 1.4–2.0 and an altitude range of 45,000–50,000 ft.[6]

This paper discusses the second phase of the F-16XL-2 project, in which an active glove flown on the left wing at supersonic, high-altitude flight conditions demonstrated the feasibility of laminar flow control for the proposed HSCT. Unlike the active glove used on the F-16XL-1 airplane, this glove was optimized for laminar flow and had variable hole spacing. Team members from the NASA Dryden Flight Research Center (Edwards, California), NASA Langley Research Center (Hampton, Virginia), Boeing Commercial Airplane Group (Seattle, Washington), McDonnell Douglas Corporation (Long Beach, California) and Rockwell International (Seal Beach, California) supported this project. The F-16XL-2 airplane was partly chosen as the flight research vehicle because its planform (70-deg inboard wing sweep), maximum speed (Mach 2.0), and maximum altitude (55,000 ft) are similar to the planform, desired cruise speed (Mach 2.4), and cruise altitude (60,000 ft) of the HSCT (fig. 1). Although the F-16XL aircraft has similar properties to the proposed HSCT, some peculiarities in this experiment are specific to the F-16XL-2 airplane and would not be of concern if the HSCT uses this technology.

The necessary F-16XL-2 modifications included the installation of a titanium glove on the left wing of the aircraft, the extension of the leading-edge region to continue the 70-deg inboard wing sweep into the fuselage (fig. 2), and the installation of a suction pump to act as the suction source for the experiment. The objectives of the flight experiment were to achieve 50- to 60-percent–chord laminar flow on a highly swept wing at supersonic speeds and to validate the tools used in the design of this experiment.

Forty-five flights were conducted at NASA Dryden in support of this experiment. This paper discusses research variables that directly impacted the ability to obtain laminar flow and the techniques used to correct for the variables in flight. These variables included flight conditions, suction, and unique F-16XL-2 shock systems.

AIRCRAFT DESCRIPTION

The F-16XL-2 aircraft was selected for this experiment because of its similarity to the proposed HSCT in both its planform (fig. 1) and maximum attainable flight conditions. The F-16XL aircraft has a double-delta-wing configuration and is a modification of the standard F-16 airplane. The wing leading-edge sweep is 70° and 50° in the inboard and outboard regions, respectively.

The F-16XL-2 airplane was the second F-16 airplane modified by General Dynamics (Fort Worth, Texas). The two-seat aircraft is capable of cruising at Mach 2.0 and an altitude of 55,000 ft when powered by the F110-GE-129 engine (General Electric, Evandale, Ohio). Figure 2 shows the left wing of the aircraft modified with a laminar flow control glove.

EXPERIMENT DESCRIPTION

Several components, discussed in the following sections, were required to ensure a successful F-16XL-2 laminar flow experiment. These components included the design flight conditions and pressure distribution, a wing glove, a suction system, shock fences, a turbulence diverter, and preflight and postflight monitoring of excrescences.

Design Flight Conditions

The design point of the experiment was selected based on computational fluid dynamics and previous transition flight experiments. The design point, Mach 1.9 at an altitude of 50,000 ft, was still within the F-16XL-2 flight envelope after the airplane was modified for this experiment. Depending on drag and engine performance, Mach numbers and altitudes higher than the design point could be achieved. The calculated Reynolds number at the design condition was 2.25×10^6, which was a function of the local temperature at altitude and varied for each flight. The design angles of attack and sideslip were 3.3° and 0°, respectively.

Design Pressure Distribution

The design pressure distribution over the wing included the components required to minimize transition-causing disturbances. The steep leading-edge acceleration to the wing upper surface allowed a rapid progression through the region of crossflow. The acceleration was followed by a gradual, favorable pressure gradient, which acted to stabilize Tollmien-Schlichting disturbances. Moreover, the lack of span-wise gradients in the design pressure distribution allowed for nearly unswept isobars on the upper surface at the design angle of attack.[7]

Although the design pressure distribution was instrumental in obtaining laminar flow, suction was required to obtain extensive laminar flow on the highly swept wing. To obtain the necessary suction, extensive F-16XL-2 modifications were made that were unique to the experiment.

Wing Glove

A perforated wing glove was installed on the left wing of the F-16XL-2 airplane. This glove and its fairing were designed by Boeing using a "constrained direct iterative surface curvature" inverse design method (developed by NASA Langley) coupled with a three-dimensional, thin-layer Navier-Stokes flow solver.[7] The glove, which Boeing also fabricated, was constructed of 0.040-in.–thick titanium perforated with more than twelve million laser-drilled holes. These holes nominally were 0.0025 in. in diameter and had a varied spacing range of 0.010–0.055 in., depending on the required suction porosity. The appendix provides further details. The conically shaped holes provided the perforated surface through which the boundary-layer instabilities were removed.

The glove was a shell that encompassed the left wing, not a replacement to the original wing. The suction panel had a 0.5-in. leading-edge radius and extended 17 ft along the leading edge and back to 60-percent chord. The suction panel was bounded by the apex, an aluminum substructure with a carbon-fiber cover; and a carbon-fiber passive fairing that blended the panel with the existing wing contour. Support structures (apex region) were added that continued the 70-deg swept wing into the fuselage (fig. 3). With these modifications, the F-16XL-2 left wing better modeled the proposed HSCT wing.

Suction System

The design suction distribution was derived by Boeing using linear, boundary-layer–stability-theory calculations. This analysis was correlated with wind-tunnel and flight transition data and used to establish the criteria for the maximum and minimum suction levels.[7]

A suction control system was designed to achieve the design suction distribution as closely as possible while applying suction to the panel surface at different levels and locations. Figure 4 shows a schematic of the suction system. Suction was provided for this system by a modified Boeing 707 cabin air–pressurization turbocompressor located in the ammunition drum bay. The rate of air drawn through the suction-panel holes was measured by mass flow sensors and controlled by butterfly flow control valves (FCVs), which then led into a common chamber, the plenum. From the plenum, air passed through a large duct where the master FCV was located. When insufficient quantities of air were drawn through the master FCV, a surge valve opened to provide supplemental air to the turbocompressor, which was nominally driven by engine-bleed air. All air exiting the turbocompressor was then vented overboard, on the right side of the aircraft.

The suction panel was divided into 20 regions, 13 of which were located in the leading edge. Three flutes, compartments created by fiberglass dividers, provided suction to those regions located in the leading edge. Figure 5 shows the four suction regions fed by each flute. Each of the 20 regions had its own mass flow sensor and FCV. A setting of 0° represented a closed valve; a setting of 90° represented a completely open valve.

The suction control system controlled the master FCV and the 20 FCVs through a computer onboard the aircraft. This computer interfaced in real time the uplinked command signal from the control room with the FCVs and set the suction levels for the 20 regions. The FCVs in each region were individually controlled, which allowed for different suction settings within each region. This system permitted several suction distributions to be studied during a given flight.

Shock Fences

Because of the engine-inlet configuration of the F-16XL-2 airplane (fig. 6), some concern existed that inlet-generated shocks could impact the leading edge of the glove, reducing the possibility of obtaining laminar flow in the affected region. To address this concern, a 20-in.–tall, vertical shock fence was installed on the lower surface of the left wing at butt line (*BL*) 65. The shock fence was mounted at a weapons ordnance hard-attachment point to block the potential engine-inlet shocks.

Figure 7 shows the two shock-fence designs flown during the experiment. The shock-fence designs, designated by the sweep angle the shock-fence leading edge made with the vertical, were constructed of aluminum and monitored for strain.[8] The first fence flown was the 60-deg shock fence (fig. 7(a)). This fence was based on a 10-in.–tall design flown during the previous phase of the F-16XL-2 laminar flow project.[6] The 60-deg shock fence was flown on 19 flights of this experiment. The second fence flown was the 10-deg shock fence installed for 24 of the research flights (fig. 7(b)). The 10-deg sweep of this fence yielded a supersonic leading edge.

Turbulence Diverter

Figure 8 shows a turbulence diverter that was installed inboard of the suction panel at the leading edge. The turbulence diverter was a passive device used to create a laminar attachment line on the glove. The diverter consisted of a narrow (0.78-in. width) longitudinal slot on the leading edge just inboard of the suction panel. This slot allowed the turbulent attachment-line boundary layer flowing outboard from the passive-fairing leading edge to be swept away and a new laminar attachment-line boundary layer to be formed on the inboard leading edge of the panel.

Three diverter configurations were flown during the previous phase of the F-16XL-2 laminar flow project. The design used for this experiment was determined to be the most effective.

Excrescences

Imperfections in the suction panel such as rough spots, dimples, and insect contamination are examples of the excrescences that can prevent a laminar attachment line. These imperfections can also cause disturbances in the boundary layer and "trip" the flow downstream of the attachment line from laminar to turbulent at the location of the imperfection. Extensive inspections were performed before and after each flight and detailed records were kept about the locations of any such excrescences. Anomalous behavior or lack of repeatability in the data occasionally was linked to these excrescences.

Before flight, the suction panel was cleaned thoroughly. Insects primarily were acquired during takeoff and landing. The condition of the insect hit allowed for the determination of "insect acquisition time" during the flight. Insects acquired during takeoff were particularly difficult to link to anomalies because they could have eroded from the surface during the flight and thus would no longer be present during the postlanding inspection. If laminar flow control were used commercially, a shield or some other type of contamination avoidance system would likely be required to protect the leading edge from insect contamination during takeoff and landing.[9]

INSTRUMENTATION

Airdata parameters were measured using a flight test noseboom designed to measure airspeed and flow angles. In addition to the dual flow-angle vanes used to measure the angles of attack and sideslip, the noseboom also provided measurements of total and static pressure. Angle-of-attack calibration data were obtained during the previous phase of the F-16XL-2 laminar flow experiment. Flow-angle accuracies were ±0.3° and ±0.5° for the angles of attack and sideslip, respectively.

The aircraft was also instrumented to measure total temperature, Euler angles, accelerations, and control-surface positions. The wing glove instrumentation consisted of pressure orifices, thermocouples, microphones, mass flow sensors, and hot-film anemometers. This paper primarily focuses on the data obtained from the hot-film anemometers.

Pressure Taps

Figure 9 shows the layout of the pressure taps on the left wing of the F-16XL-2 airplane. Both surface and internal pressure measurements were obtained during the experiment. Of the 454 surface pressure taps, 200 were located on the active suction panel, 113 of which were in the leading-edge region.

The remaining 254 surface pressure taps were located on the passive fairing, including the apex surrounding the suction panel. These taps were flush-mounted pressure orifices with an internal diameter of 0.0625 in. The 72 internal pressure taps were used to monitor the pressure within the suction flutes (fig. 9).

Mass Flow Sensors

Twenty mass flow sensors were inserted in the ducts between the suction-panel surface and the FCVs. These sensors, designed by Kurz Instruments Inc. (Monterey, California), were used to measure the suction flow rate in each region. The sensors were based on a Kurz Instruments thermal convective single-point insertion "CD"™ mass velocity sensor and consisted of a glass-coated platinum wire over ceramic sealed with epoxy.

The mass flow sensors had an accuracy of ±3 percent of the reading. Each sensor and region valve assembly used to correlate valve position with mass flow was laboratory-calibrated at NASA Langley.

Hot-Film Anemometers

Hot-film sensors with temperature-compensated anemometer systems (fig. 10(a)) were used on or around the suction panel on both the upper and lower surfaces. Hot-film sensors of this type have been used on high-performance aircraft in several experiments at NASA Dryden. The sensors were mounted such that their active elements were nearly perpendicular to the airflow, with the temperature elements adjacent and slightly aft of the hot-film sensors to avoid possible flow disturbance over the active elements of the hot-film sensors. The anemometer system compensates for the local stagnation temperature, which allows the sensors to operate in conditions where large speed and altitude variations occur.[10]

Twenty-four hot-film sensors were mounted directly to the titanium surface on the edge of the active suction region on the wing upper surface. The amount of hot films on the active suction surface varied from 0 for the first 8 flights to 31 for the final flights (fig. 10(b)). The location of these hot films varied as different areas of the suction panel were investigated. The desire to mount hot films to the active suction surface generated some concern about residue blocking the suction-panel holes. As a result, the sensors were directly mounted not to the surface, but instead to polyester tape that left no residue and was rated for high temperatures and dynamic pressures (fig. 10(b)). Before this experiment began, speed and temperature tests were performed both in flight and in the laboratory to verify that the tape could be used in this manner.

Although the number of usable lower-surface hot films was limited to 15, the location and number of these sensors also varied throughout the flight phase. Initially, 14 lower-surface hot films were used, the first of which was mounted to the carbon-fiber panel just forward of the turbulence diverter. The other 13 were mounted directly to the titanium surface on the edge of the suction-panel regions. Figure 11 shows the 146 hot-film locations studied throughout the flight phase. The number of hot-film anemometry cards available in the instrumentation system limited the number of recorded hot films to 50 preflight-determined hot films.

Data Recording

All instrumentation data were telemetered to the control room in real time during the research flights and recorded. The airdata and aircraft parameters were measured at 50 samples/sec. The research

pressure data were obtained at 12.5 samples/sec. Mass flow data were obtained at 60 samples/sec. The telemetered hot-film data were acquired at 100 samples/sec. Hot-film data were also recorded on a 14-track magnetic tape drive using frequency modulation and constant bandwidth. These high-frequency data were recorded at 2 and 10 kHz during the program; however, the results presented in this paper were derived from the telemetered data because transition was easily observed at that frequency. Hot-film signals were measured in volts and telemetered to the control room, which allowed decisions regarding flight-maneuver quality to be made in real time.

The hot-film sensor signal used in this experiment had both direct-current (steady-state) and alternating-current (dynamic) components. In previous NASA Dryden experiments, these components were separated and recorded as two signals.[11] Boundary-layer state classification requires both components to obtain the best results. For this experiment, the two components were recorded as one signal.

Figure 12 shows a hot-film signal under a laminar boundary layer that has turbulent bursts bounded by a signal from a turbulent boundary layer at the beginning and the end. The top curve shows the combined signals; the second curve shows the direct-current (steady-state) component of the signal; and the bottom curve shows the alternating-current (dynamic) component of the signal. This combination signal eliminated some confusion and made boundary-layer state classification an easier process.

Interpretation of Hot-Film Signals

Hot-film sensors were used to determine the boundary-layer state. Figure 13 shows typical hot-film signals and their boundary-layer state designation. The dynamic portion of the hot-film signal was "quieter" for laminar flow than for turbulent flow because the temperature-compensated hot-film sensors required less voltage input to keep the temperature constant for laminar flow. Laminar flow required less voltage because of little mixing in the boundary layer and therefore less convective heat transfer away from the sensor existed than for turbulent flow. Consequently, the signal had a low amplitude. Conversely, for turbulent flow where heat-transfer rates increase and rapidly fluctuate because of large mixing in the boundary layer, higher voltage was required and the signals had a higher amplitude.

The steady-state portion of the hot-film signal was characterized by a voltage offset. This offset was a lower voltage for hot films in areas of laminar flow as opposed to turbulent flow. High-amplitude spikes were an indication of transitional flow. Spikes in the direction of positive voltage indicated a mostly laminar signal with turbulent bursts. Spikes in the direction of negative voltage indicated a mostly turbulent signal with laminar bursts. Peak transition was indicated by a maximum occurrence of high-amplitude spikes.[11, 12]

TEST CONDITIONS

Data were obtained throughout each research flight; however, the results presented in this paper primarily were obtained at flight conditions of Mach 2 at altitudes ranging from 50,000 ft to 55,000 ft, angles of attack ranging from 2.0° to 4.0°, and angles of sideslip of either 0.0° or 1.5° nose right. Several disturbances occurred, which will be discussed in the "Results" section, that led to the maneuvers

primarily being conducted at these flight conditions instead of the design conditions of Mach 1.9, an altitude of 50,000 ft, 3.3° angle of attack, and 0.0° angle of sideslip.

The design conditions were determined from previous flight results and analysis of computational fluid dynamics results. The desired angles of attack and sideslip were based on the cruise conditions of the HSCT (3.5° and 0.0° angles of attack and sideslip, respectively). The maneuvers typically performed were steady-state pushovers to a predesignated angle of attack. These pushovers were performed with and without sideslip and were approximately 10 sec in duration.

RESULTS

The flight test results presented consist primarily of boundary-layer transition data obtained from hot-film sensors. In the following sections, pressure distributions, the variables that affect the attachment line, suction effects, and the extent of laminar flow obtained are discussed.

Shock Fence

Two distinct shocks emanated from the engine inlet. One shock came from the inlet diverter, and the other came from the inlet face (fig. 14(a)). During the previous F-16XL-2 flight tests,[6] a 10-in.–tall version of the 60-deg shock fence was flown to reduce the effect of the inlet-diverter shock on the wing leading edge. Because of the partial effectiveness of that fence, a 20-in.–tall fence was designed for this experiment to provide better protection. As will be shown, the 20-in.–tall, 60-deg fence was effective at blocking the inlet-diverter shock, which resulted in a desirable pressure distribution on the leading edge. However, the fence was unable to block the shock off the inlet face, which was further forward (fig.14(a)). This shock was not identified in earlier flight tests because the gloveless wing leading edge was further inboard and aft.

The sweep angle of the 10-deg shock fence was designed to more effectively block both shock structures and prevent shock spillage; however, the supersonic leading edge of this fence produced a shock of its own. The resulting expansion altered the leading-edge pressure data, which is exactly what the shock fences were designed to prevent. Two flights were flown without either shock fence installed to confirm the necessity of the shock fence and obtain baseline data.

Pressure Distributions

The pressure distribution over the suction glove was measured at constant intervals from *BL* 50 to *BL* 110. Several variables influenced the glove pressure distribution, including engine-inlet shock and canopy-joint shock disturbances (fig. 14). Figure 14(b) shows the canopy-joint shock impingement on the left wing. Figure 15 shows pressure-distribution data for the suction panel. The data are graphed as coefficient of pressure (C_p) as a function of chord location (x/c) for flight at Mach 2.0.

The open symbols (fig. 15) represent pressure results from flight with the 10-deg shock fence installed. The test condition shown is the maximum laminar flow test point (0.46 x/c), which occurred at an altitude of 53,000 ft, 3.7° angle of attack, and –1.5° angle of sideslip. The solid symbols (fig. 15) represent pressure results from flight with the 60-deg shock fence installed. This test condition resulted in

laminar flow to 0.42 x/c, which occurred at an altitude of 53,000 ft, 3.4° angle of attack, and –1.5° angle of sideslip. This case was the maximum run of laminar flow with the 60-deg shock fence installed. The "X" symbols (fig. 15) represent pressure results for a test point without the shock fence installed, which occurred at an altitude of 50,000 ft, 3.7° angle of attack, and 0.0° angle of sideslip. No laminar flow was achieved during this test condition, and no test points were flown at 53,000 ft without the shock fence installed.

Figure 15 shows pressure-distribution plots for *BL* 50–100. Both the 10-deg shock-fence data and no shock-fence data were taken at 3.7° angle of attack and generally show good agreement. The 60-deg shock-fence data, taken at a slightly reduced 3.4° angle of attack, has slightly higher upper-surface pressure coefficients. Shock impingement on the glove upper surface was characterized by an adverse pressure gradient, indicating increased pressure in the affected region. The engine-inlet shock had a sharp peak because it was a strong shock. The canopy-joint shock was weaker, so the change in the pressure coefficient was not as large. The circled pressure data (fig. 15) define the locations on the upper surface of the suction panel of impingement caused by the two shock-generating systems.

Figures 15(a) and (b) show pressure-distribution data for *BL* 50 and *BL* 60. The canopy-joint shock is visible at *BL* 60. The lower-surface and leading-edge pressures predictably show excellent agreement because these butt lines are inboard of the engine-inlet shock impingement on the leading edge. The canopy-joint shock is visible for the data from flight with the 60-deg shock fence installed, but not for the other cases at *BL* 60. The lack of canopy-joint shock presence at *BL* 60 is most likely caused by the small angle-of-attack difference between the test points, which can shift the shock to 0.2 x/c, a location of no pressures.

Figures 15(c) and (d) show the pressure-distribution data for *BL* 70 and *BL* 80. Both shock-generating systems were identified from data for the three shock-fence configurations. At *BL* 70, the agreement between the 60-deg shock-fence pressure data and data from flight without a shock fence installed indicates the inlet shock was impacting the lower surface. The 10-deg shock-fence data are more negative at the lower surface, which indicates that the 10-deg fence was better able to block the inlet shock than the 60-deg shock fence. The shift in the lower-surface pressures for all three cases indicates the inlet shock impinges at the leading edge at *BL* 80. The canopy-joint shock is also visible for all shock-fence configurations.

Figures 15(e) and (f) show pressure-distribution data for *BL* 90 and *BL* 100. The return of lower-surface pressure agreement for all three configurations indicates that the inlet shock impingement affected the upper surface by lowering the attachment line (that is, lower pressure), and therefore the upper-surface pressures as well. For *BL* 90 and *BL* 100, the inlet shock impingement visibly affects the upper-surface pressure data of the flight without a shock fence installed. Canopy-joint shock impingement occurred on the upper surface for all three shock-fence configurations.

Attachment Line

To achieve laminar flow over a significant portion of the perforated glove, obtaining and maintaining a laminar, leading-edge attachment-line boundary layer on a highly swept wing at supersonic speeds is a primary concern. Lower-surface hot films placed near the leading edge were used to identify the span-wise extent of laminar flow at the attachment line.

Many variables affect the attachment-line–boundary-layer state. Three of these variables—flight conditions, the shock fences, and the turbulence diverter—contributed to the difficulty in obtaining a laminar attachment line and are discussed in the following subsections.

Flight Condition and Shock-Fence Effects

Key parameters in laminar flow experiments are Reynolds number, angle of attack, and angle of sideslip. Figures 16–18 show conditions where a laminar attachment line was obtained as a function of various flight parameters. The data were acquired at a Mach range of 1.9–2.0 and an altitude range of 50,000–55,000 ft. The symbols (figs. 16–18) represent the test points where all lower-surface hot films were laminar, indicating a laminar attachment line. The data are further defined by shock-fence configuration. Triangles represent data from flights when the 60-deg shock fence was installed, and circles represent the 10-deg shock-fence data. The reason for two shock-fence designs was based on their influence on the attachment line. A completely laminar attachment line was not attainable without a shock fence installed because of the inlet shock effects (discussed in the Shock Fence Results subsection). During the two flights without a shock fence installed, 2.9° was the maximum angle of attack for which the lower-surface hot films inboard of the shock-fence location were laminar. The outboard lower-surface hot films were not expected to be laminar because no shock fence was installed to keep the engine-inlet shock from impacting the attachment line.

Figure 16 shows the data plotted as unit Reynolds number (Re/ft) as a function of angle of attack (α). The best repeatable laminar flow results achieved at a desirable angle of attack occurred at 3.7° angle of attack for a unit Reynolds number of 2.23×10^6/ft. During these research flights, a unit Reynolds number of 2.23×10^6/ft was most often attained at Mach 2.0 and an altitude of 53,000 ft. The attachment-line laminar flow results were very sensitive to angles of attack and sideslip. Investigation with the 10-deg shock fence installed proved that a laminar attachment line could be achieved for angles of attack as high as 3.7°. Figure 17 shows angles of attack and sideslip plotted for this test condition. Both positive (nose left) and negative angles of sideslip were investigated. A laminar attachment line could not be achieved for positive angles of sideslip. Although a laminar attachment line could be obtained for 0° angle of sideslip, the most successful laminar flow results repeatedly were obtained by "unsweeping" the left wing to –1.5° angle of sideslip (fig. 18).

Turbulence Diverter Effects

Preflight predictions indicated local upper-surface streamlines such that turbulent wedges from the inboard row of hot films would not contaminate hot films downstream. However, the inboard region of the suction-panel upper surface (fig. 11) was always turbulent. This turbulent boundary layer was postulated to have been formed because the turbulence diverter was not removing all of the oncoming turbulent flow, thus preventing a laminar boundary layer from being formed in the inboard suction-panel regions. Moreover, the turbulence diverter may also have been generating a vortex that would cause turbulent flow along the inboard edge of the glove.

To verify this theory, the turbulence diverter was filled with low-density foam and room-temperature vulcanizing silicon 4130, and coated with epoxy (fig. 19). When filled, the turbulence diverter was no longer able to remove the turbulent boundary layer to allow a laminar attachment line to form. Instead, the attachment line was completely turbulent, regardless of suction distributions or flight conditions. The hypothesis then was that both the turbulence diverter and the canopy-joint shock were the cause of the

turbulent inboard upper-surface region. The forward portion of the turbulent inboard region was most likely caused by a vortex generated by the turbulence diverter. The aft portion of the turbulent inboard region was a high-crossflow region caused by the shock off the canopy joint discussed in the Pressure Distribution Results subsection.[7]

Suction Effects on Transition

To achieve laminar flow, the experiment used FCVs in the ducts to actively control suction on the perforated suction glove. Obtaining the optimum suction distribution over the panel was extremely important and challenging. Figure 20 shows the design suction distribution at Mach 1.9 and an altitude of 50,000 ft. Figure 20 also shows a flight suction distribution that repeatedly yielded successful laminar flow results at Mach 2.0 and an altitude of 55,000 ft. The flight suction values in flute 1 represent the laminar attachment-line, flight-determined optimum suction level. A laminar attachment line could not be obtained for suction coefficient values in excess of these values, which were usually less than design in the attachment-line regions.

Evidence that the design levels may have been too high in the attachment-line regions was obtained when the suction system was turned off. Because the suction system usually was not turned on until the aircraft was nearing the flight test conditions, time existed to observe the behavior of the hot films with the suction off. The lower-surface hot films located span-wise between the turbulence diverter and the shock fence were often laminar without suction at altitudes and Mach numbers ranging from 45,000 to 50,000 ft and 1.69 to 1.93, respectively. Figure 21 shows examples of this phenomenon. These sensors became turbulent when design suction was turned on because of too much suction in the attachment-line regions. However, preflight predictions had shown the design suction level necessary to overcome the leading-edge pressure disturbance from the inlet shock. This need for lower-than-design suction occurred only on the attachment line; hot films in the other suction regions could be laminar with design suction. In fact, suction in the remaining leading-edge regions was set at levels higher than design (fig. 20) to compensate for the limited levels in the attachment-line regions.[7]

Figures 22–26 show examples of the effectiveness of these and other suction settings in flight at a speed of Mach 2.0 and altitudes ranging from 53,000 to 55,000 ft. The data are from the wing glove with the 10-deg shock fence installed and from hot-film sensors indicating the boundary-layer state for a specific suction distribution. The comparison plots (figs. 22–26) were compiled from several flights, and the hot-film layout varied from flight to flight. The boundary-layer state in a specific region varied as suction changed within that region.

In the attachment-line regions, the FCVs were all set to the same flight values as those shown in figure 20, with some variation for region 11. Any disparity in the mass flow (that is, the suction coefficient) for constant valve settings were caused by changes in flight condition. Throughout the flight experiment, the suction valve in region 20 was closed and no hot films were placed on the suction-panel surface in that area, because laminar flow was not expected to be seen. Note that, when shown, the upper-surface hot films inboard of the suction-panel regions are always turbulent, as mentioned in the Turbulence Diverter Effects Results subsection.

Figure 22 shows three cases that demonstrate the effect of glove suction variation on the lower-surface hot films (that is, the attachment-line–boundary-layer state). In these cases, suction

variations occur in all regions except regions 1, 2, 5, and 8, located at the attachment line. The variations in region 11, also located at the attachment line, indicate that the three hot films furthest aft on the lower surface (closest to region 11) were affected. Although the suction in region 11 (figs. 22(a) and (b)) was essentially the same, the turbulent-with-laminar-bursts signal on the outboard leading edge (fig. 22(a)) occurred because the suction in flutes 2 and 3 was not enough, as compared to that in figure 22(b), to sustain the laminar flow conditions on the panel. Figure 22(b) shows the effectiveness of maximum suction in the leading-edge regions, (that is, the FCVs in those regions were open the maximum amount, 90°). Decreasing the suction in region 11 finally produced the desired laminar attachment line (fig. 22(c)).

Figure 23 shows two suction distributions. The suction in the leading-edge regions was identical in both cases, and the lower-surface hot films indicated the same boundary-layer state for the attachment line in both test points. Figure 23 shows a comparison of the upper-surface suction settings that demonstrate the necessity of higher suction in regions 14–19. The upper-surface boundary-layer state (fig. 23(a)) was mostly turbulent with laminar bursts. Increasing the rooftop suction produced the laminar-with-turbulent-spikes signal on the upper-surface hot films (fig. 23(b)).

Figure 24 shows a good example of attachment-line and boundary-layer state repeatability. As in figure 23, suction variations occurred only in the rooftop regions. As expected, the lower-surface hot film signals were identical for both cases. The suction settings in the rooftop regions further demonstrate the necessity for higher suction in those areas in order to obtain laminar flow over a large percentage of the glove.

Figure 25 shows an indication of the lack of sensitivity of the upper-surface boundary-layer state to small variations in suction. The suction settings in the leading-edge regions were the same as in figure 24, with variation only in regions 14–19. The valves in the upper-surface regions varied from 40° (fig. 25(a)) to 45° (fig. 25(b)). The hot-film states were very similar to those in figure 24. By using a multiple-region suction coefficient ($C_{q_{MR}}$), a 13.7-percent difference exists with ±3.7-percent error in the suction distribution for regions 14–19 of the two cases. Therefore, when the suction in the leading-edge regions was held constant, the boundary layer was not very sensitive to small changes in rooftop suction. This insensitivity is further demonstrated by a comparison of figure 25(b) with figure 24(b). A 10.7-percent $C_{q_{MR}}$ difference exists with ±3.7-percent error in the suction distribution for regions 14–19 and very little variation exists in the hot-film signals.

The leading-edge suction values (fig. 26) represent the flight-determined optimum suction settings for a laminar attachment line. The large steps in suction in the rooftop regions (figs. 26(a)–(c)) demonstrate the necessity for high suction in these regions. The small FCV angles (fig. 26(a)) yielded mostly turbulent hot-film signals, but the hot films in figure 26(b) indicate more laminar signals for a 20-deg change in FCV position. The suction distribution shown in figure 26(c) is the same flight distribution shown in figure 20; valves in the rooftop regions are open to 90°. This distribution also yielded a laminar attachment line and laminar flow in the rooftop regions. The turbulent and turbulent-with-laminar-bursts signals in region 15 were caused by the existence of the hot-film sensors mounted forward of the sensors in region 14.

Extent of Laminar Flow

When all of the attachment-line variables were taken into account and the suction system had been exercised and its limits understood, the extent of laminar flow could be maximized. Figures 27 and 28 show two cases that document the long runs of laminar flow achieved at Mach 2 during the course of the program. The figures show the wing glove with hot-film sensors that indicate the state of the boundary layer for a specific suction distribution. The shaded area represents the region of laminar flow over the wing glove. In both cases, all the lower-surface hot films were laminar, indicating a laminar attachment line. The suction distribution for each case, including the design suction, is also shown. As in the distribution from figures 20 and 26(c), maximum suction was employed in flutes 2 and 3 and in the rooftop regions, with suction variation occurring only for the attachment-line regions. A 45.3-percent $C_{q_{MR}}$ difference exists with ±3.3 percent error between the flute 1 suction distributions of the two cases. Both of the cases shown were obtained with the 10-deg shock fence installed.

In figure 27, the laminar flow region is bounded by turbulent and laminar-with-turbulent-bursts hot-film signals. The hot film furthest aft to indicate laminar flow for this test point was located at 0.41 x/c, which made the maximum laminar flow distance a minimum of 8.60 ft. This location corresponds to a Reynolds number of 21.2×10^6 at 2.6° angle of attack and 0.0° angle of sideslip. The attachment-line suction distribution was not the flight-determined optimum discussed in the Suction Effects on Transition Results subsection. However, a laminar attachment line was still attainable because of the low angle of attack, which was lower than the desired HSCT cruise angle of attack.

Figure 28 shows the laminar flow region bounded by turbulent and transitional hot-film signals. This test point occurred at 3.7° angle of attack (closer to the desired HSCT cruise angle of attack than those of figure 27), –1.5° angle of sideslip, and a Reynolds number of 22.7×10^6. The hot film furthest aft to be laminar was located at 0.46 x/c, which made the laminar flow distance 10.30 ft. Except for the very small variation in region 11, the suction distribution shown is identical to those shown in figures 20 and 26(c).

These long runs of laminar flow were not the only cases. In fact, a very good example of repeatability occurred on the last flight where 14 test points consistently demonstrated laminar flow as far aft as 0.42 x/c. All of these cases occurred at Mach 2.0 and an altitude of 53,000 ft; used the attachment-line flight-determined optimum suction levels; and had variation occur only in flutes 2 and 3 and in the rooftop regions. Unfortunately, the direct-current level of several hot-film sensors was out of range on that flight, so the actual extent of laminar flow was unknown.

CONCLUDING REMARKS

A titanium, laminar flow control glove with variable hole spacing has been flown on the left wing of the F-16XL-2 aircraft. Boundary-layer transition data have been obtained on this glove primarily at Mach 2.0 and altitudes of 53,000 to 55,000 ft.

Best results have been obtained at Mach 2.0 and an altitude of 53,000 ft rather than the design Mach number and altitude (Mach 1.9 and 50,000 ft, respectively). At an angle of attack (3.7°) near the desired cruise angle for the High-Speed Civil Transport (HSCT), laminar flow was obtained to a minimum 0.46 chord location (x/c) corresponding to a Reynolds number of 22.7×10^6. Laminar flow has been consistently obtained to a minimum 0.42 x/c with the flight-determined optimum suction levels.

Reducing suction levels at the attachment line from the design levels was necessary to obtain a laminar attachment line. However, increasing the suction levels above design on the rest of the panel was required to maximize the laminar flow conditions further aft.

Shocks peculiar to the F-16XL-2 airplane caused some compromises in the experiment. Shocks off the inlet required a shock fence to be installed on the lower surface of the left wing and the airplane to be flown at an angle of sideslip of 1.5° nose right. At times, a shock off the canopy joint resulted in unfavorable pressure gradients and boundary-layer transition on the upper surface. These shocks and resulting effects would not be present on a HSCT implementing laminar flow control technology.

EC91 0646-01

(a) The F-16XL-2 airplane.

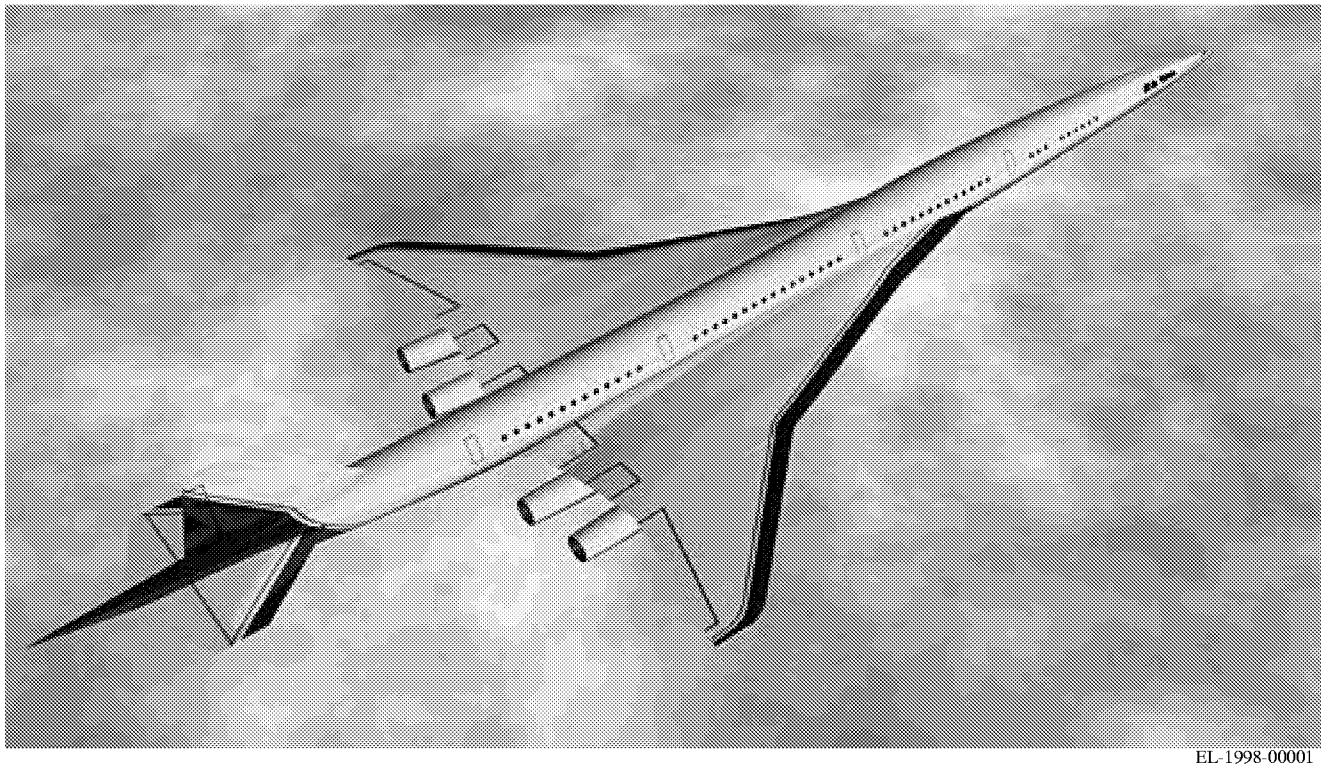

EL-1998-00001

(b) HSCT concept.

Figure 1. Comparison of the unmodified F-16XL-2 and HSCT aircraft.

EC96-43548-07

Figure 2. The F-16XL-2 dual-place aircraft with suction glove installed on left wing.

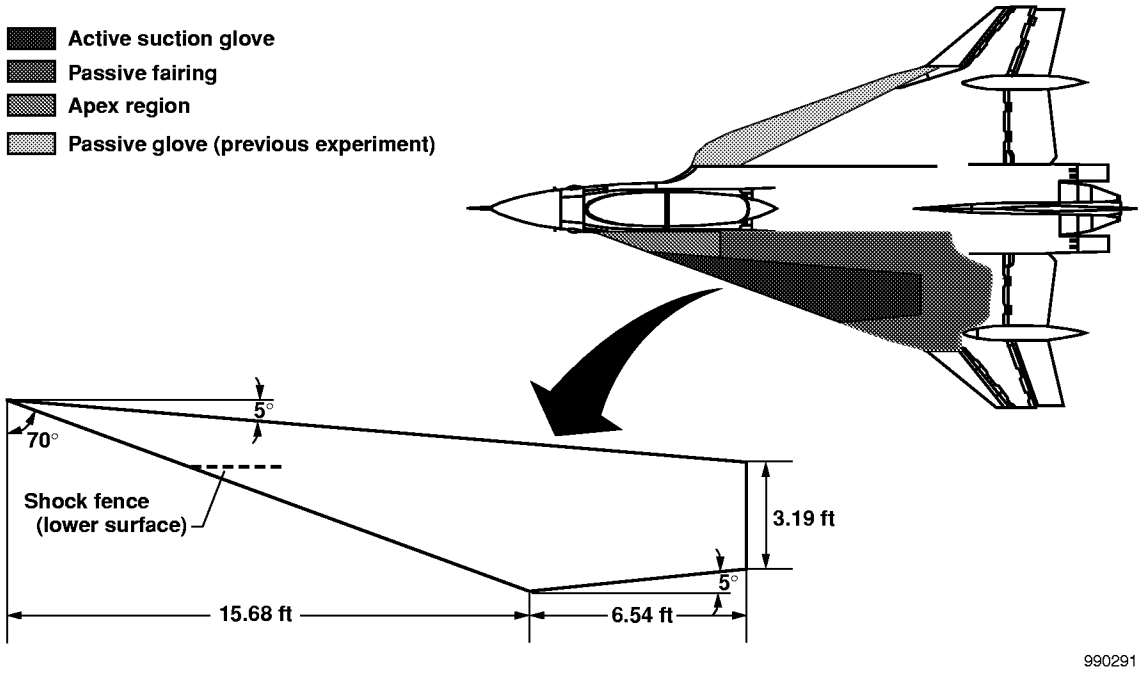

Figure 3. Aircraft configuration.

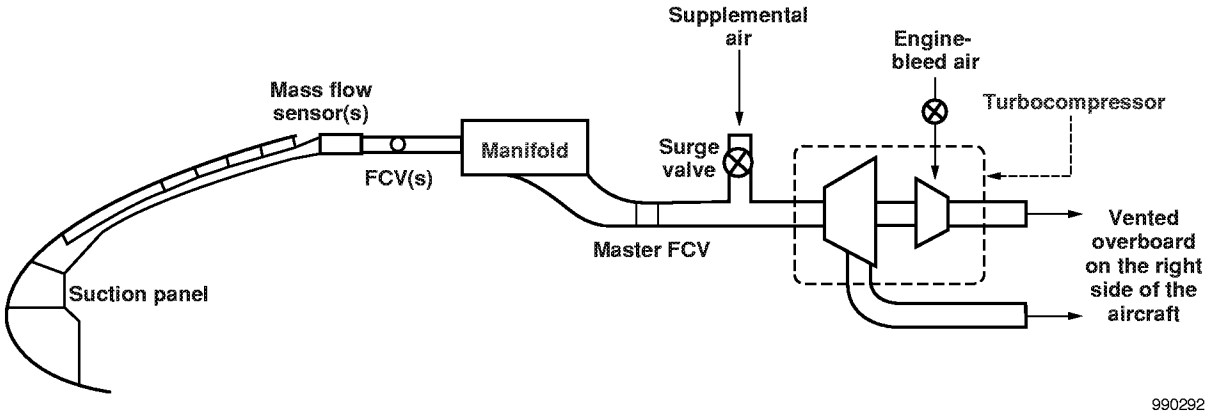

Figure 4. Suction system schematic.

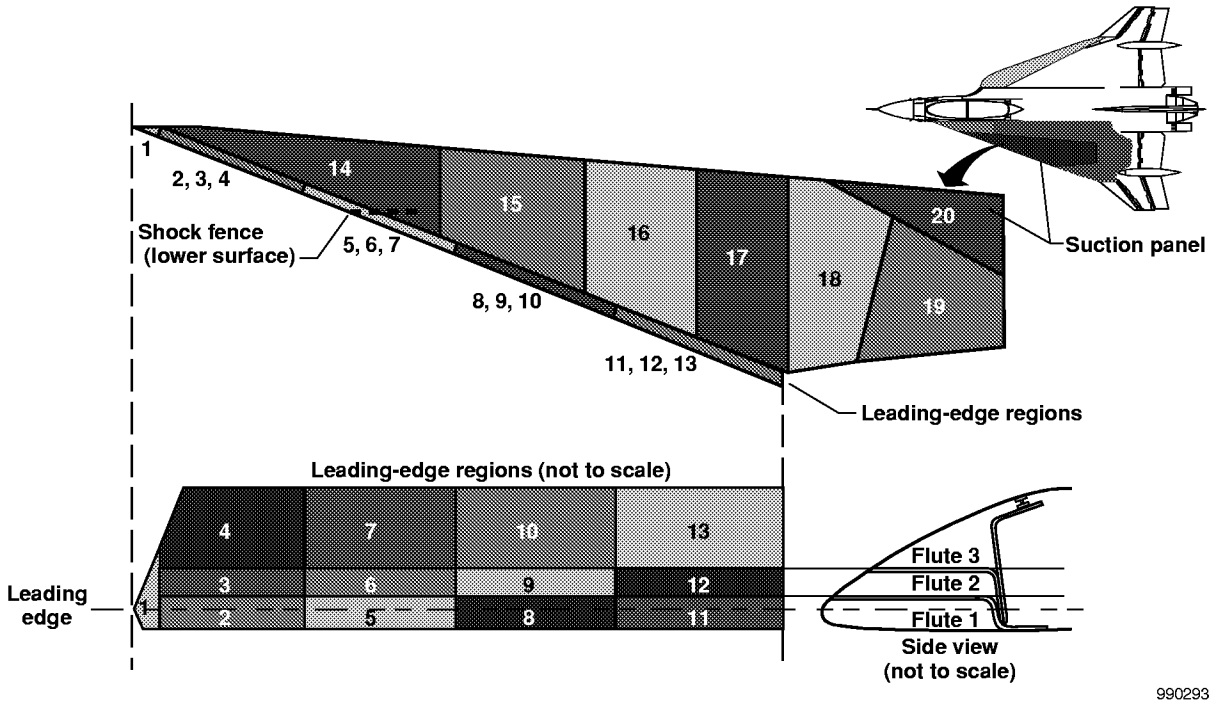

Figure 5. Suction-panel regions.

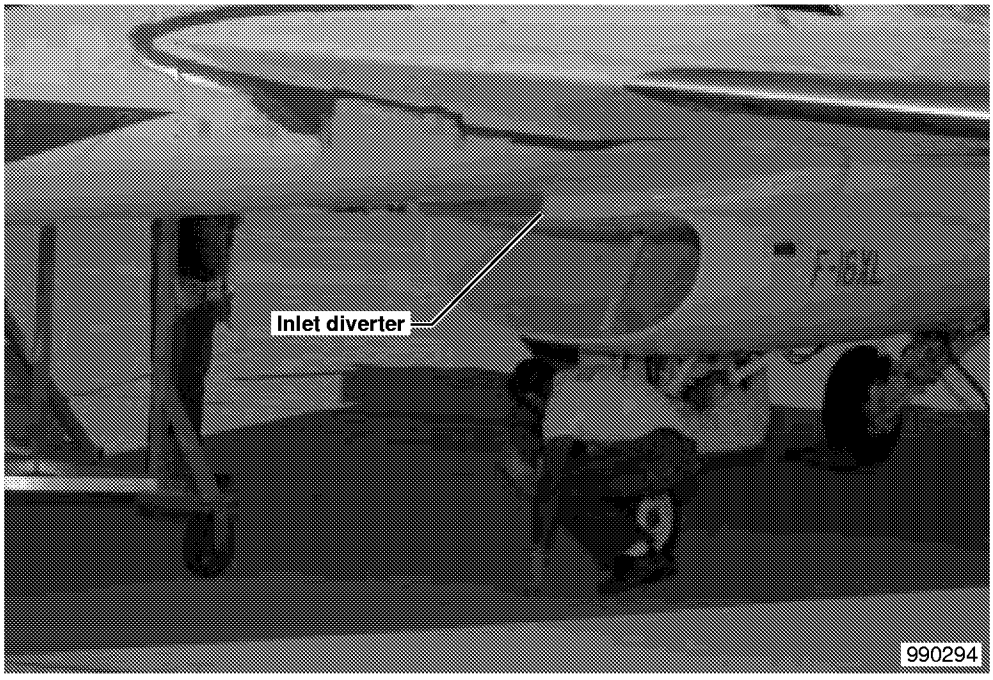

Figure 6. The F-16XL-2 engine inlet.

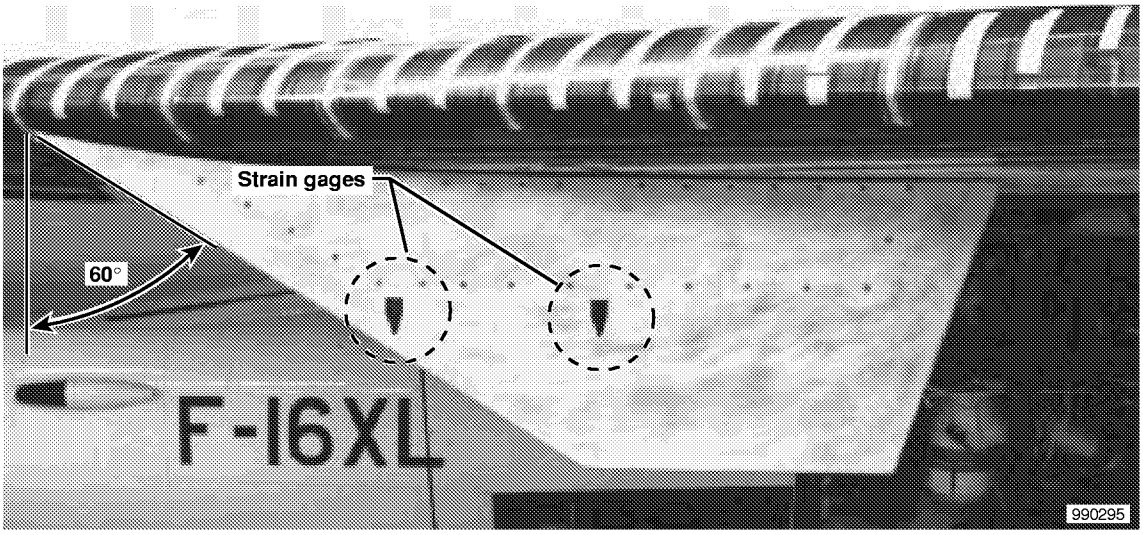

(a) 60-deg shock fence.

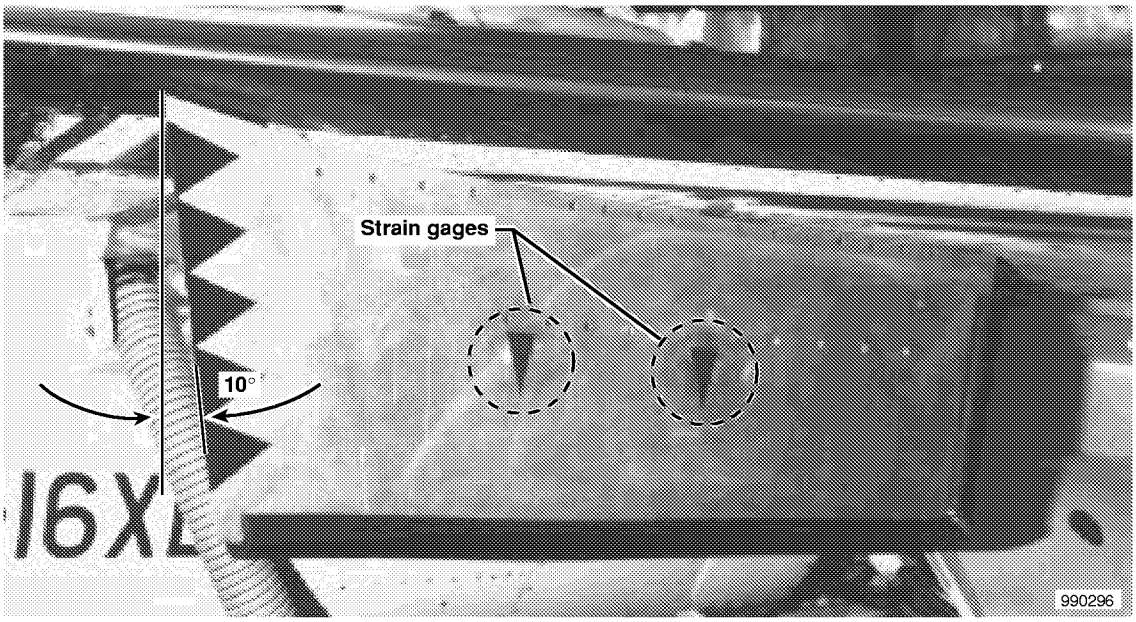

(b) 10-deg shock fence.

Figure 7. Shock-fence configurations.

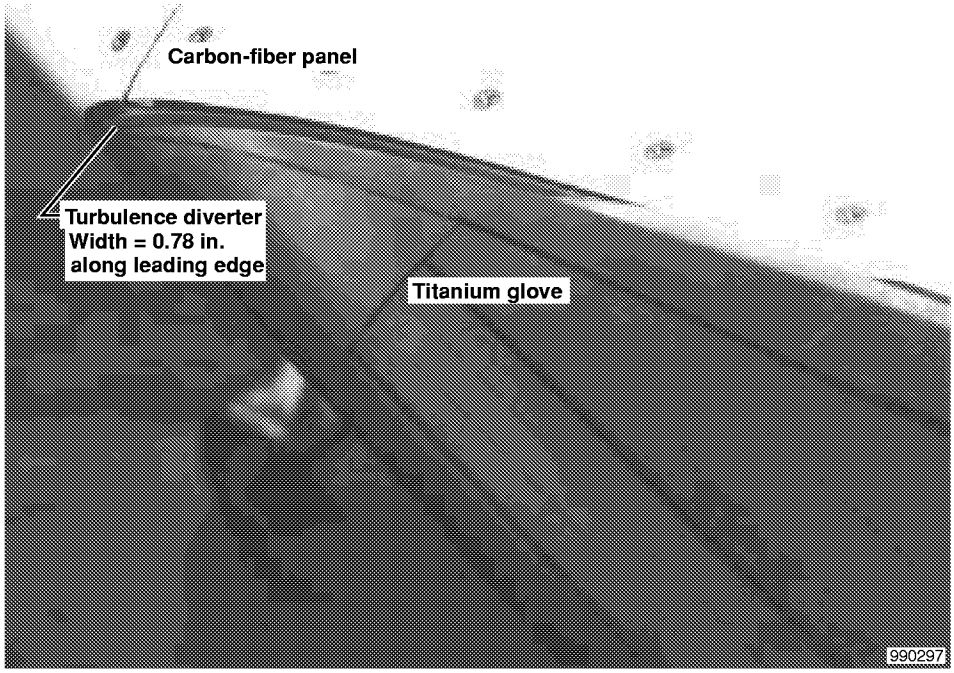

Figure 8. Turbulence diverter.

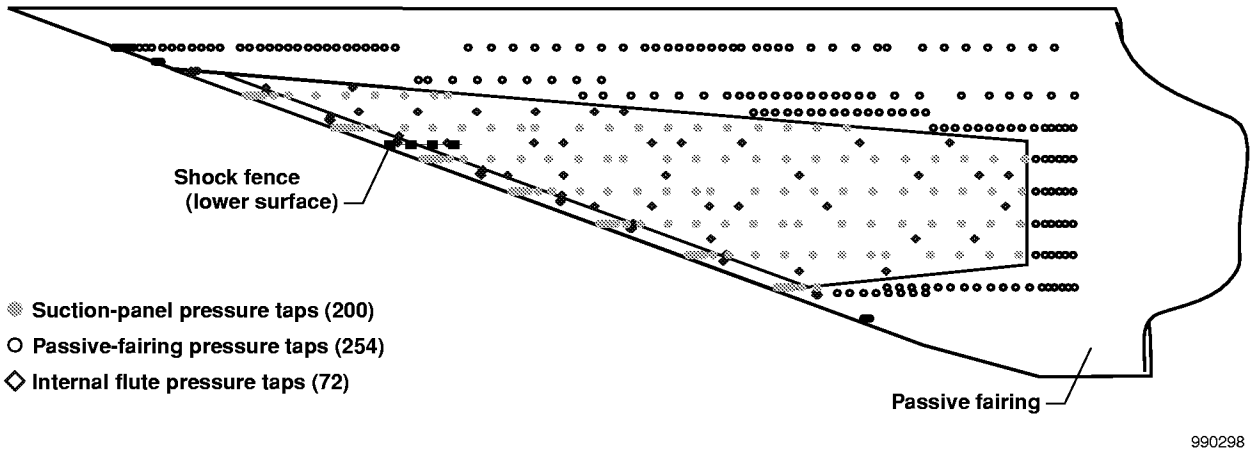

Figure 9. Suction-panel and passive-fairing pressure tap layout.

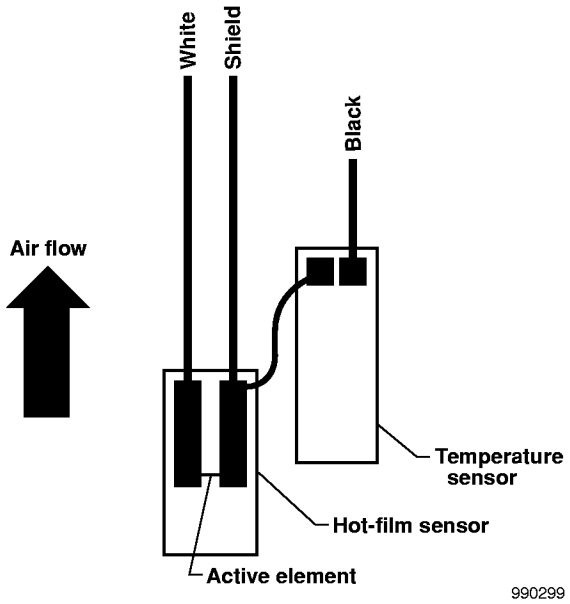

(a) Hot film.

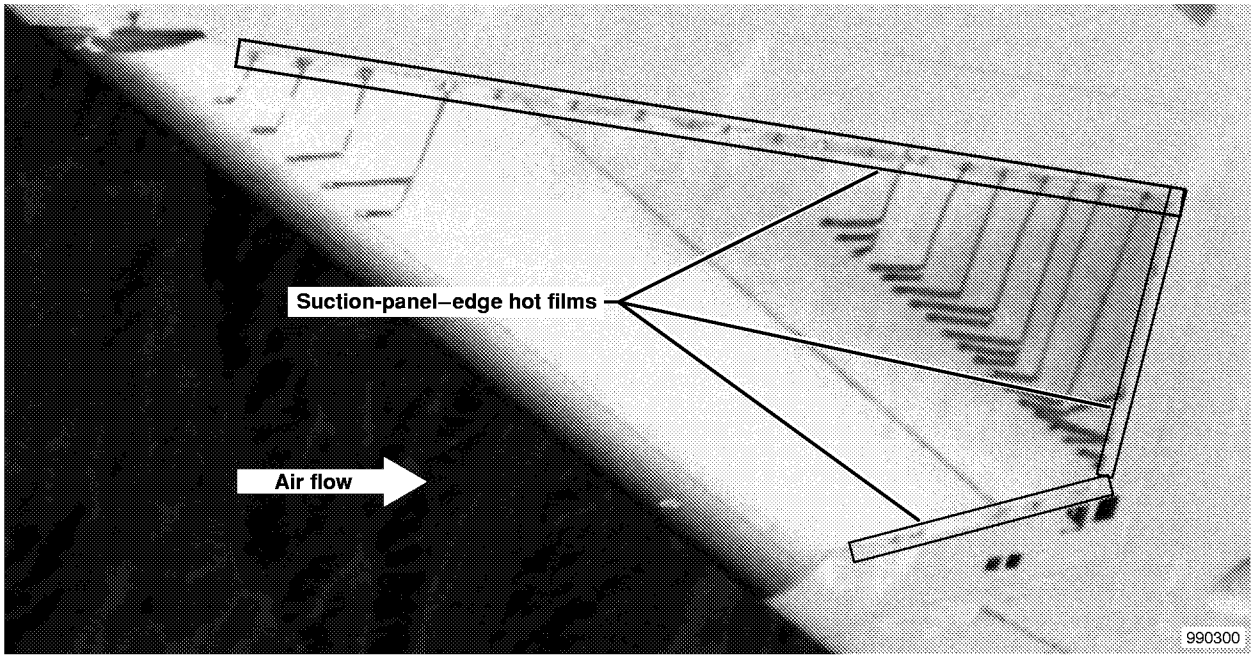

(b) Upper-surface hot films.

Figure 10. Hot-film anemometers.

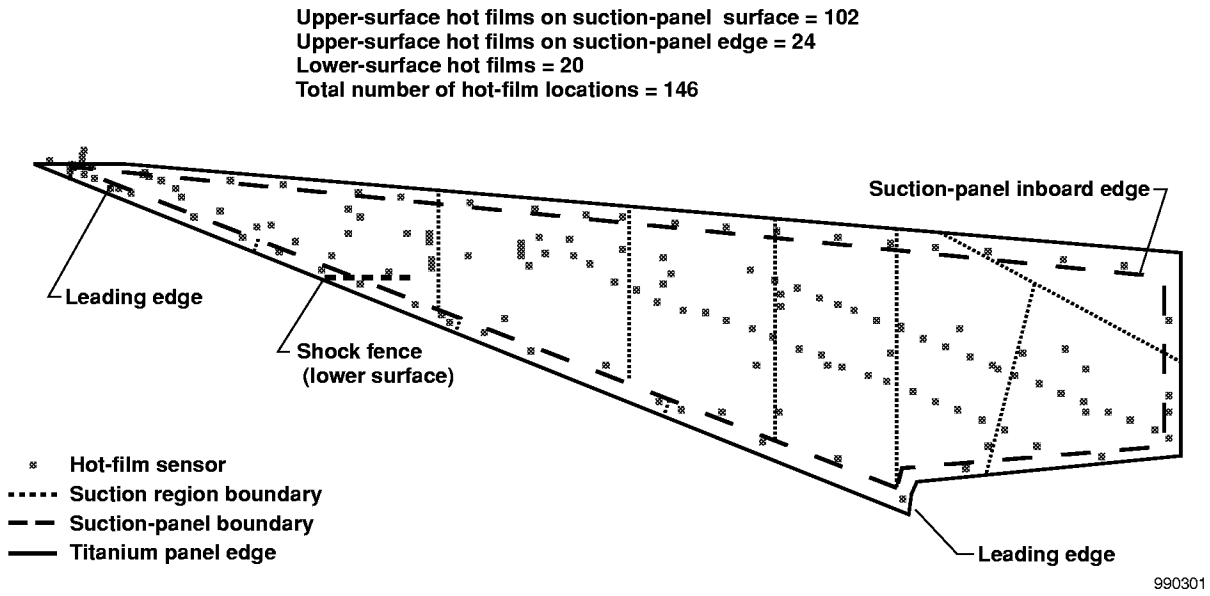

Figure 11. Hot-film locations studied.

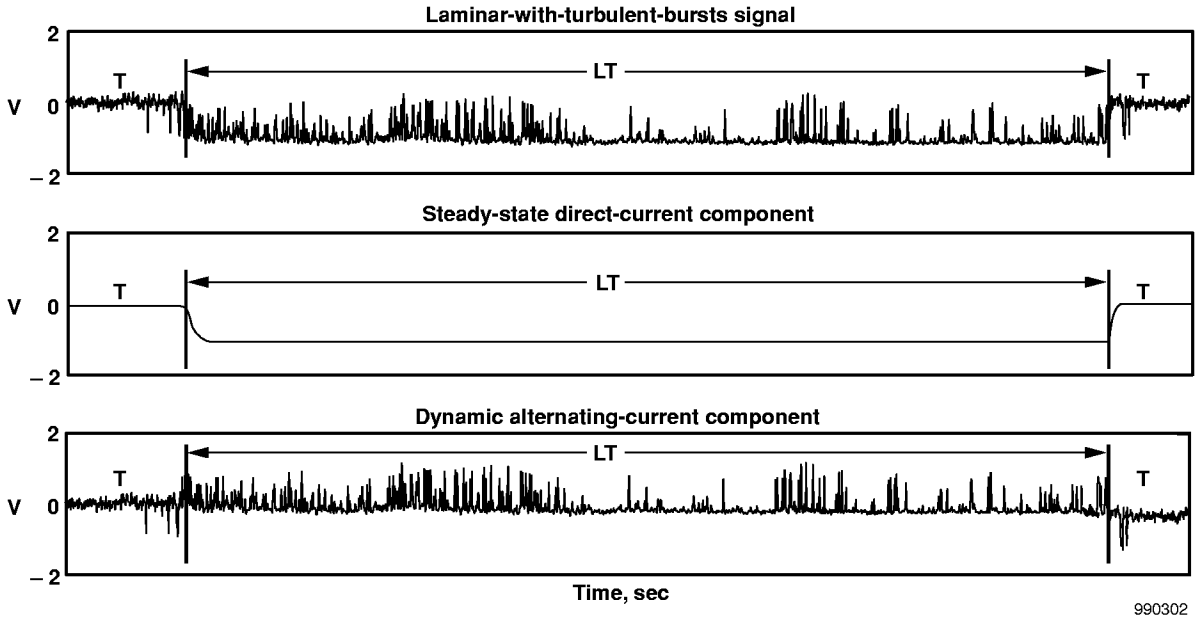

Figure 12. Hot-film signal components.

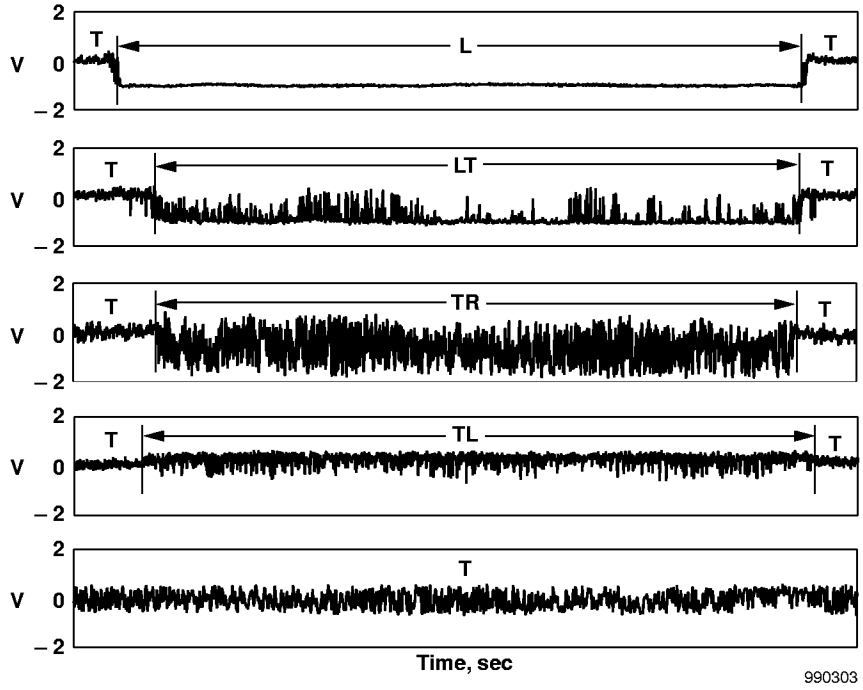

Figure 13. Hot-film signal classification.

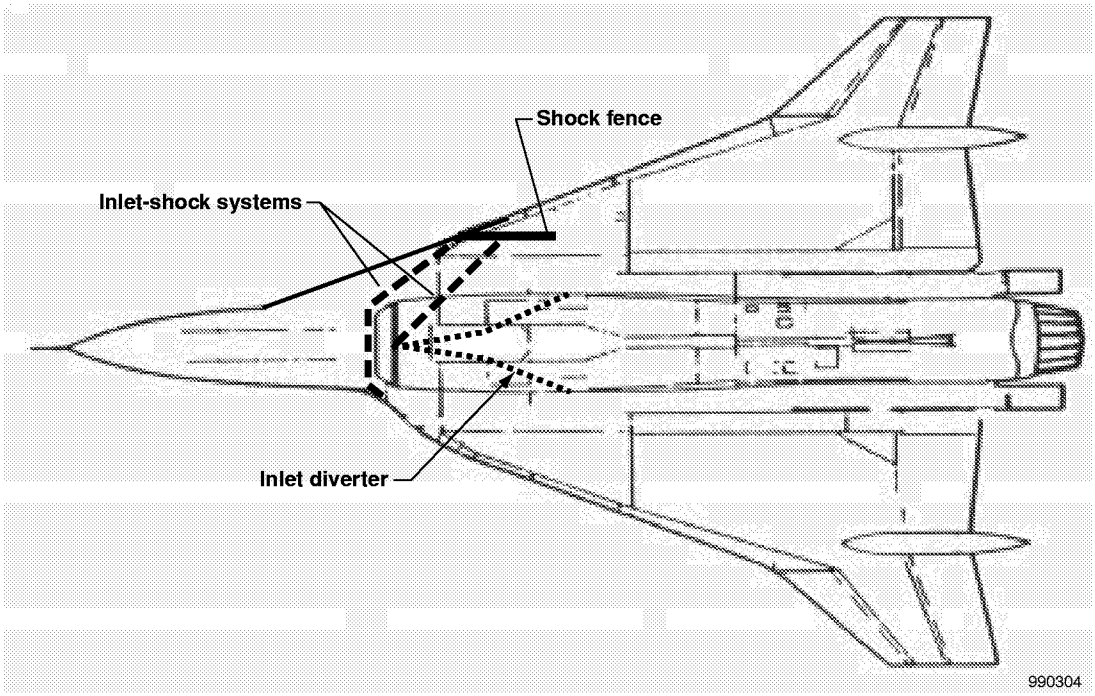

(a) Lower surface.

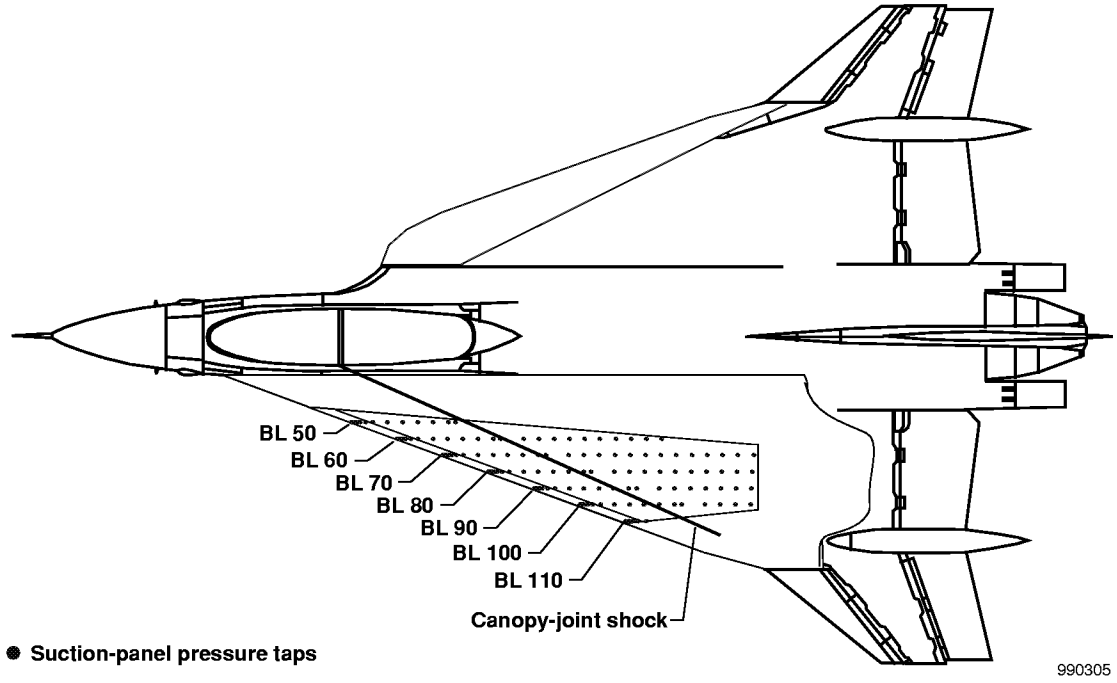

(b) Upper surface.

Figure 14. Shock disturbances.

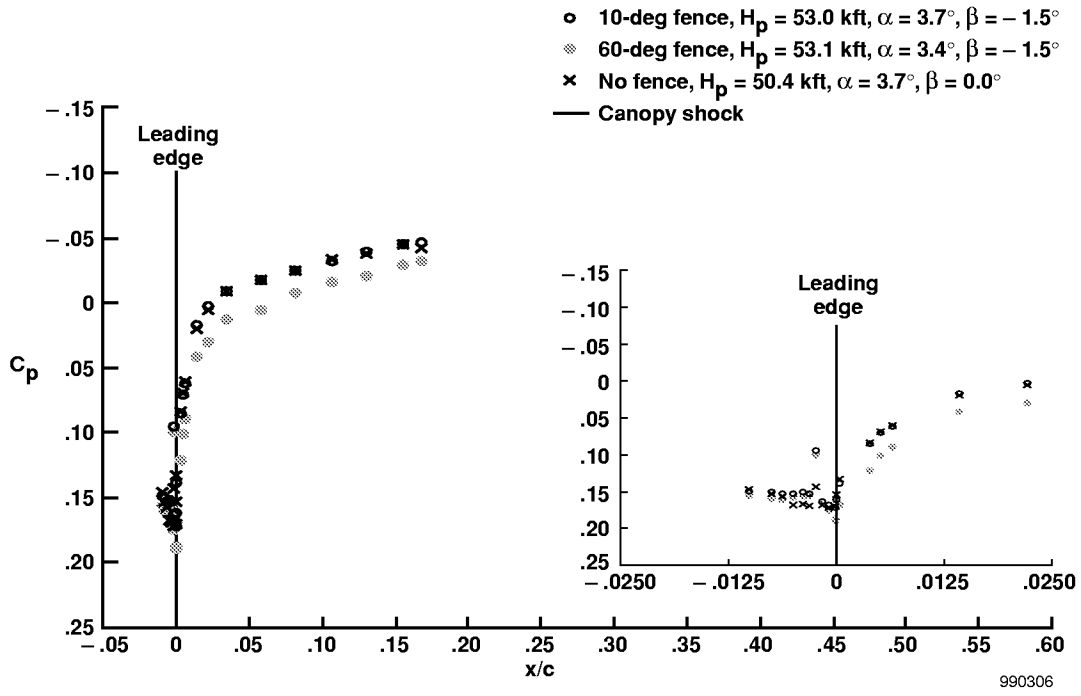

(a) *BL* 50.

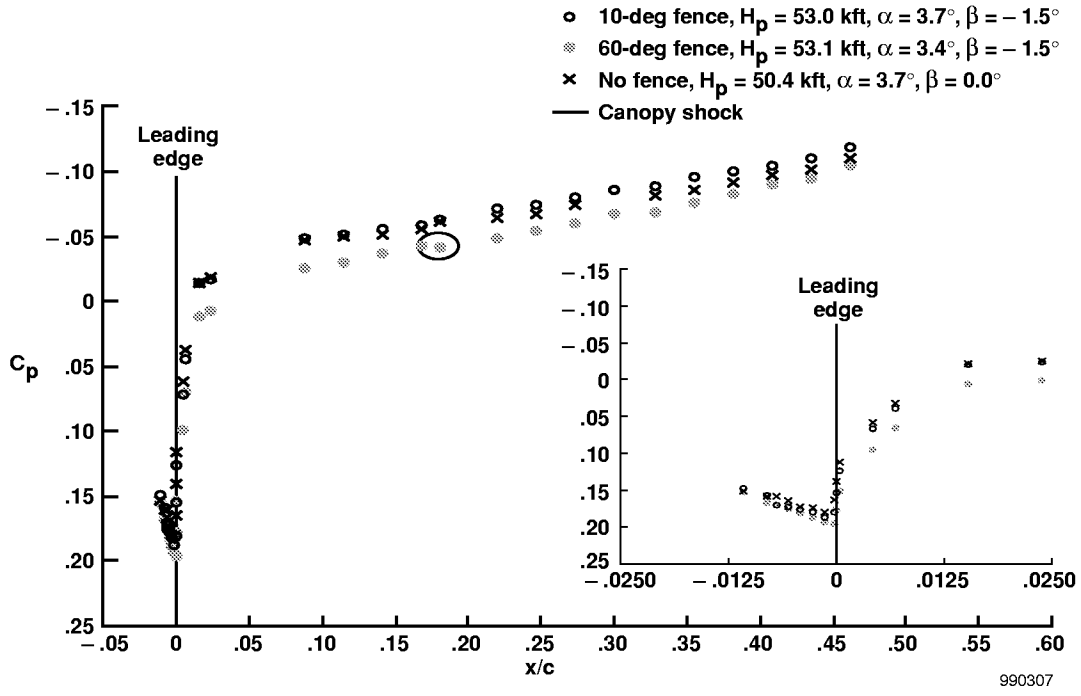

(b) *BL* 60.

Figure 15. Pressure distributions for Mach 2.0.

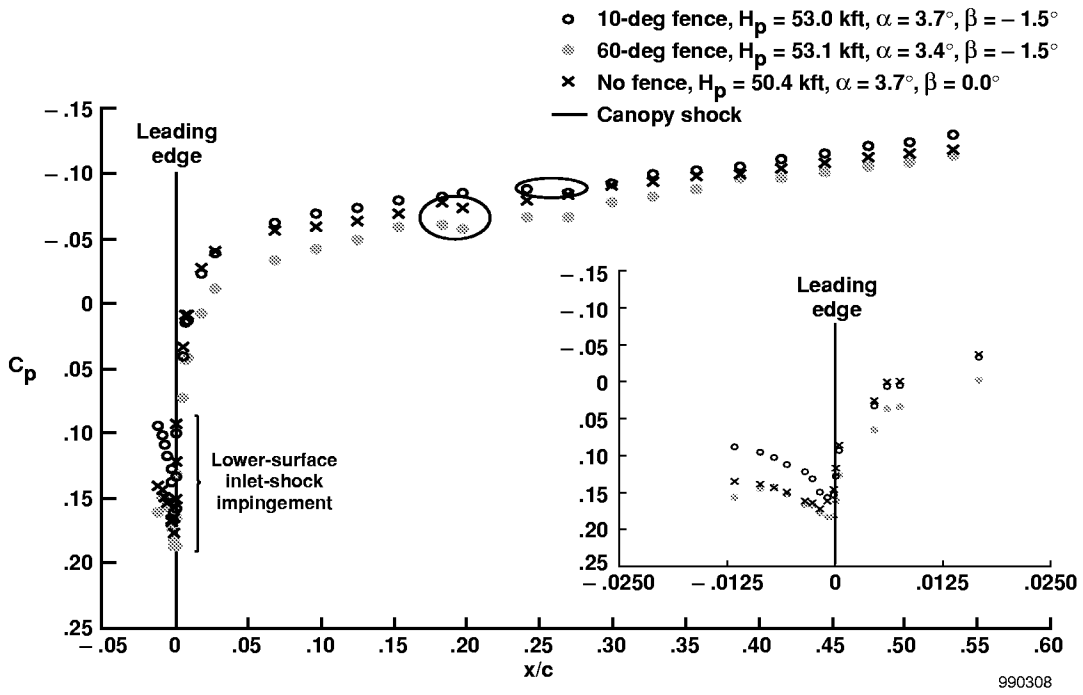

(c) *BL* 70.

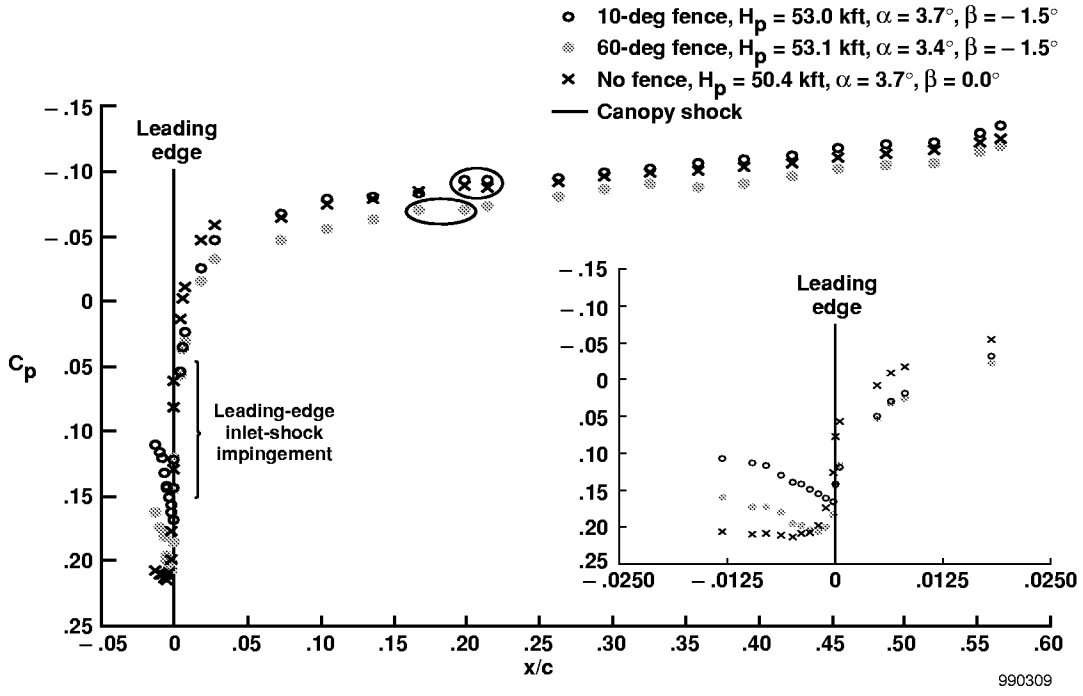

(d) *BL* 80.

Figure 15. Continued.

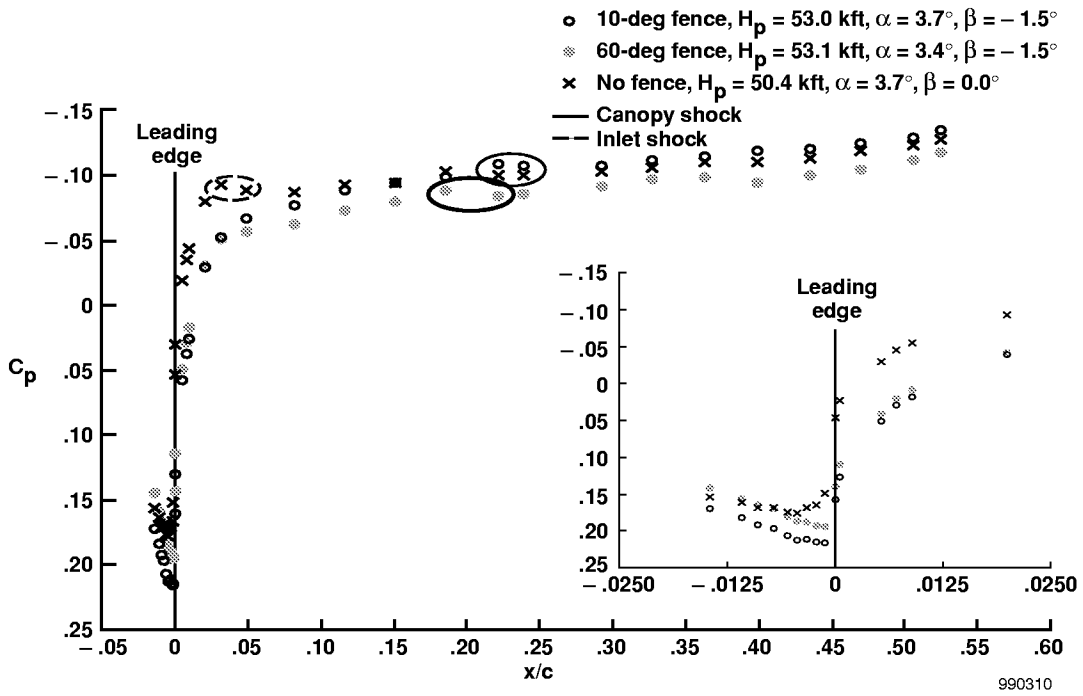

(e) *BL* 90.

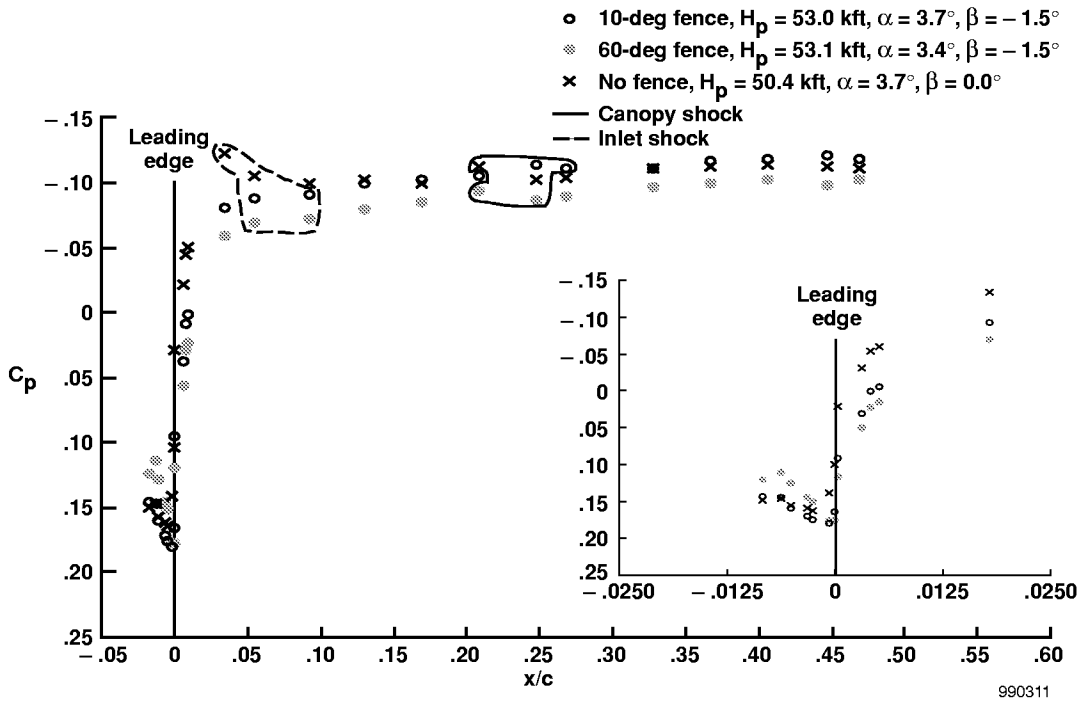

(f) *BL* 100.

Figure 15. Concluded.

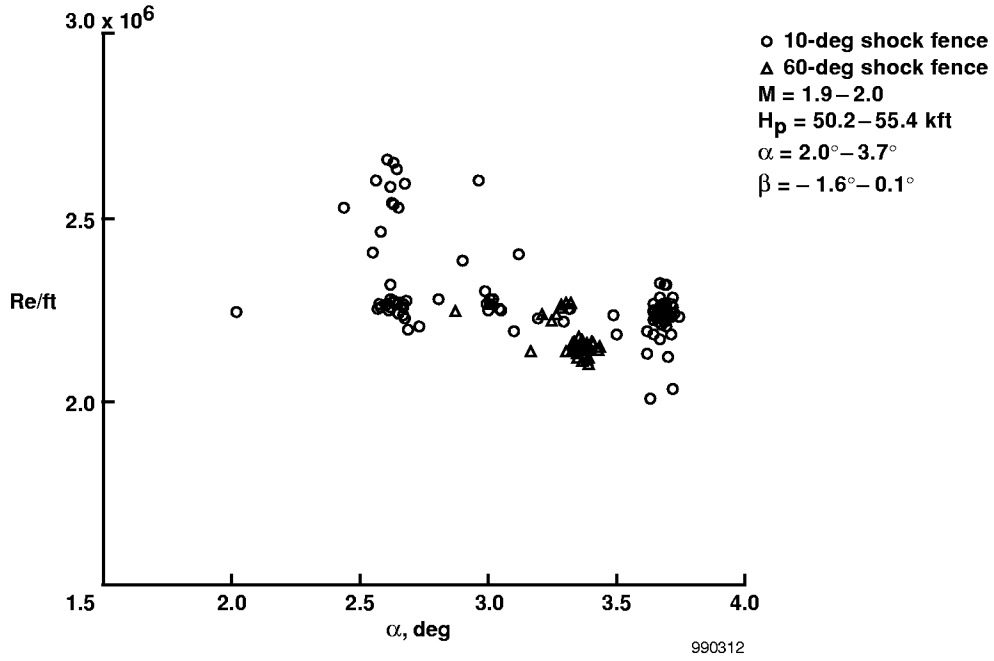

Figure 16. Reynolds number and angle-of-attack test conditions under which a laminar attachment line was obtained.

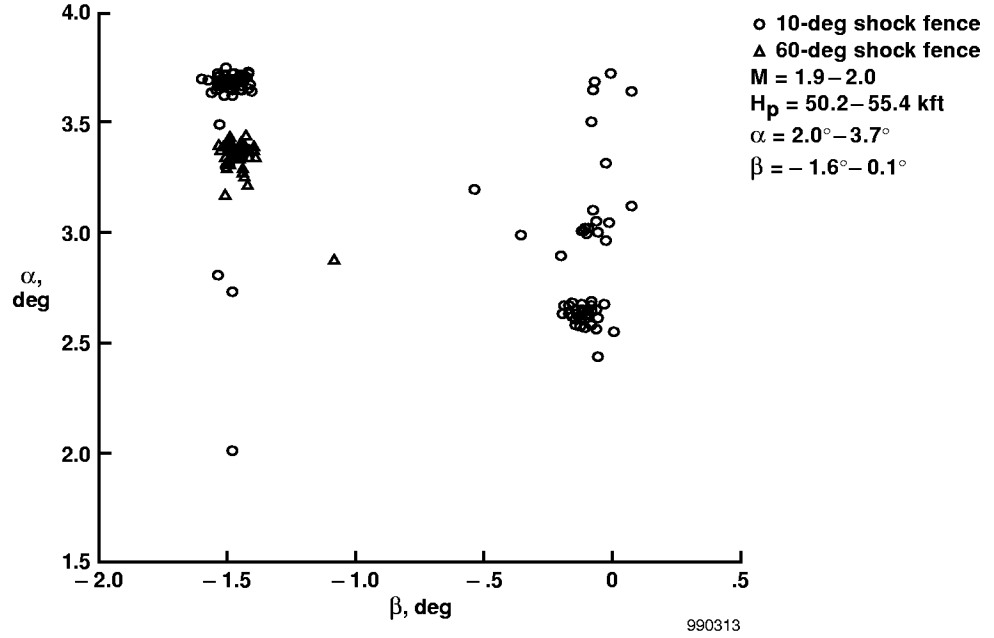

Figure 17. Angle-of-attack and -sideslip test conditions under which a laminar attachment line was obtained.

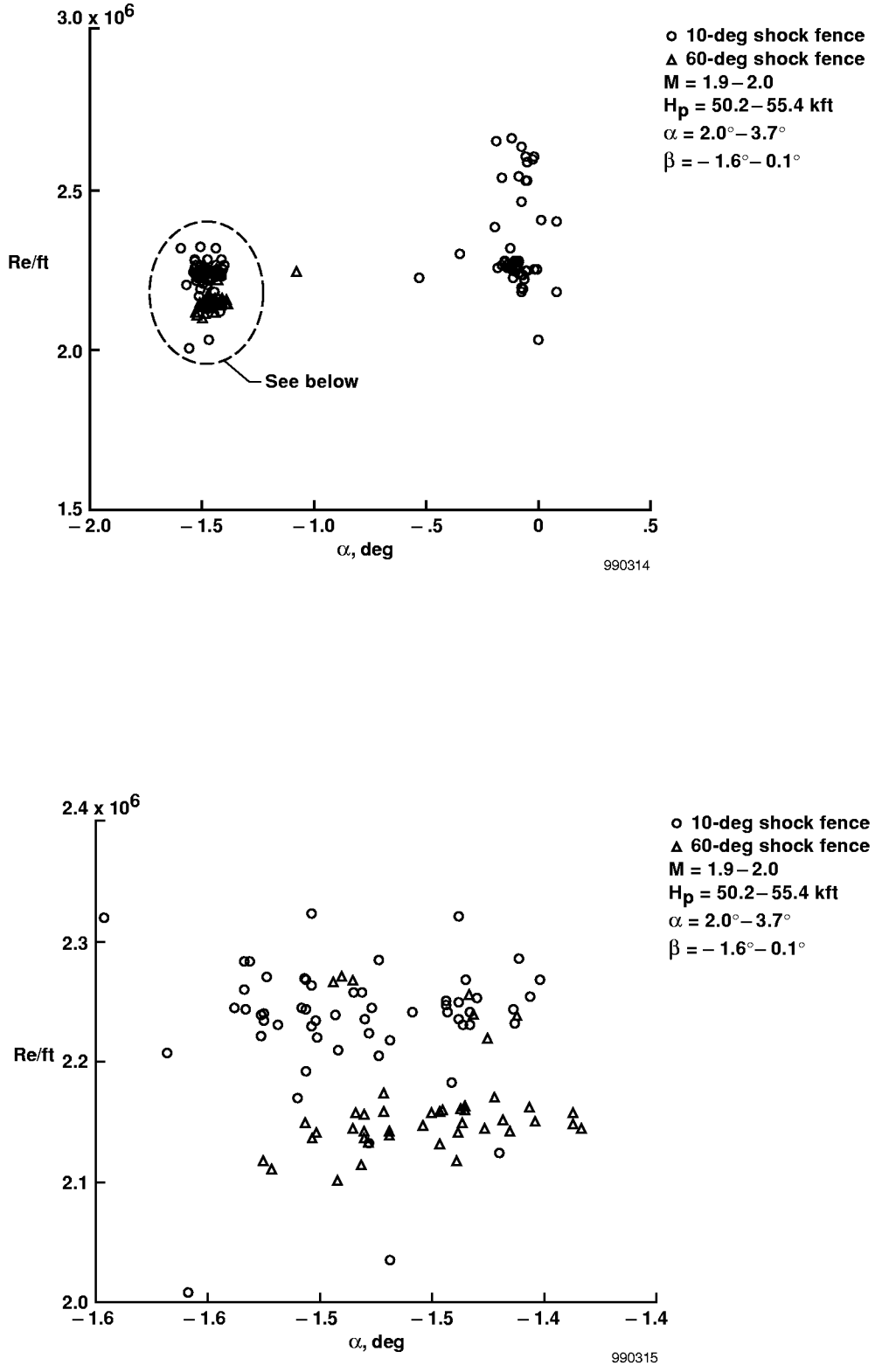

Figure 18. Reynolds number and angle-of-sideslip test conditions under which laminar attachment line was obtained.

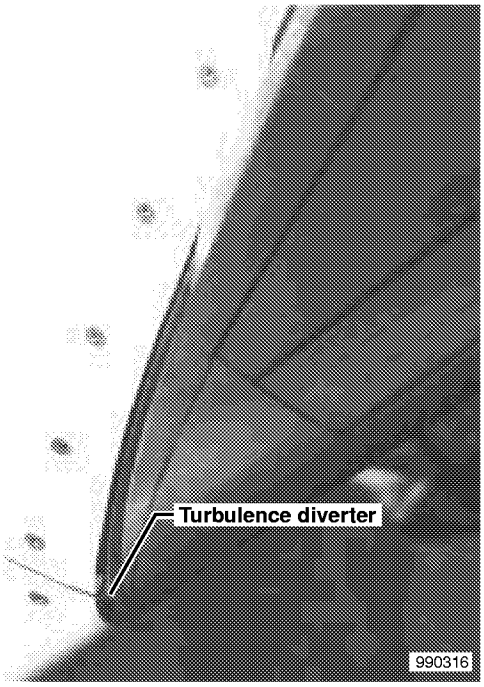

(a) Nominal.

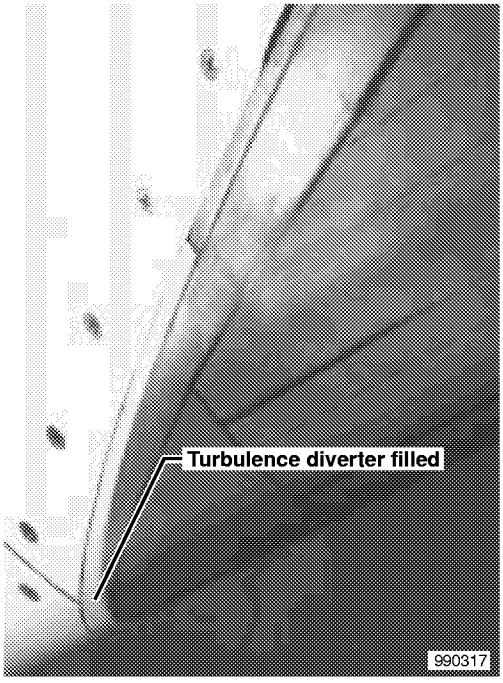

(b) Filled.

Figure 19. Turbulence diverter.

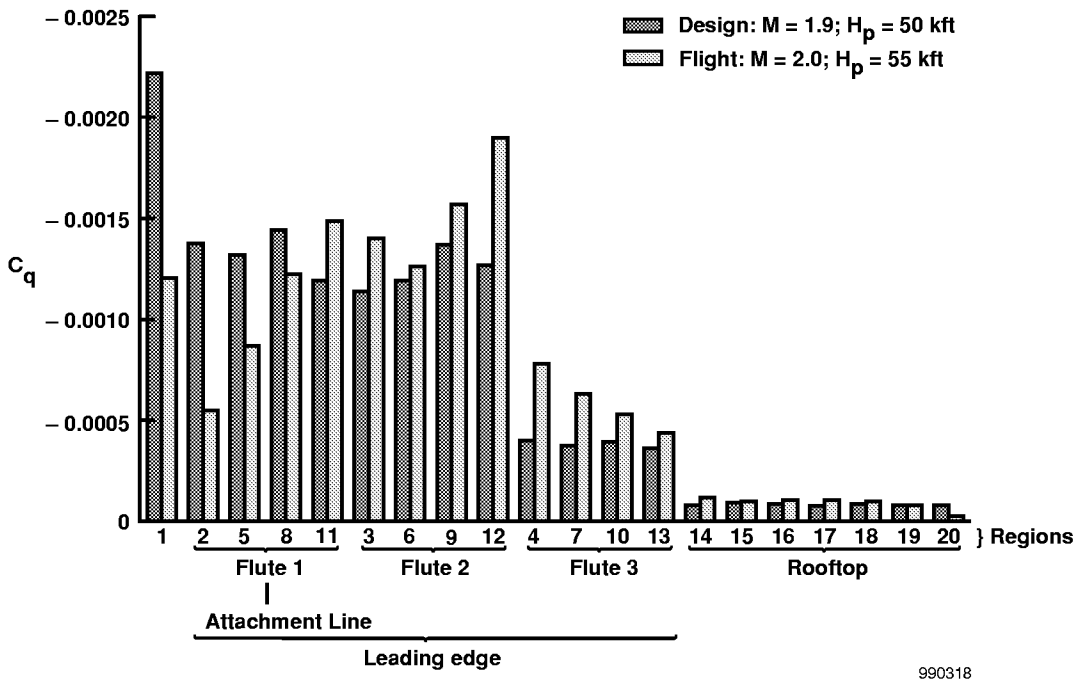

Figure 20. Suction distribution.

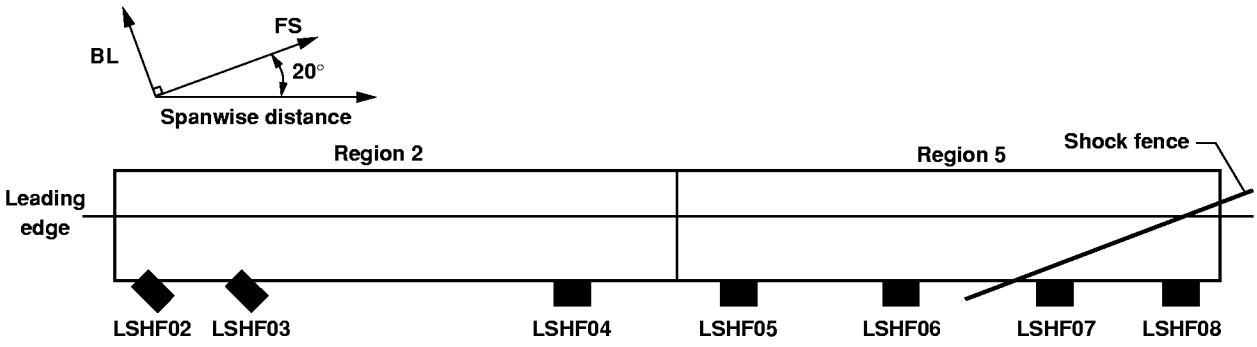

				Lower surface hot films						
M	H_p, kft	Re, mil/ft	α, deg	2	3	4	5	6	7	8
1.690	50.5	1.97	4.24	L	L	L	L	T	T	T
1.807	50.7	2.12	3.96	L	L	L	L	T	T	T
1.861	50.4	2.20	3.96	LT	L	L	LT	L	T	T
1.898	49.7	2.42	3.24	LT	L	L	LT	L	T	T
1.901	45.1	2.81	3.13	L	L	L	LT	L	T	T
1.933	50.7	2.26	3.95	L	L	L	LT	T	T	T

990319

Figure 21. Lower-surface hot films without suction.

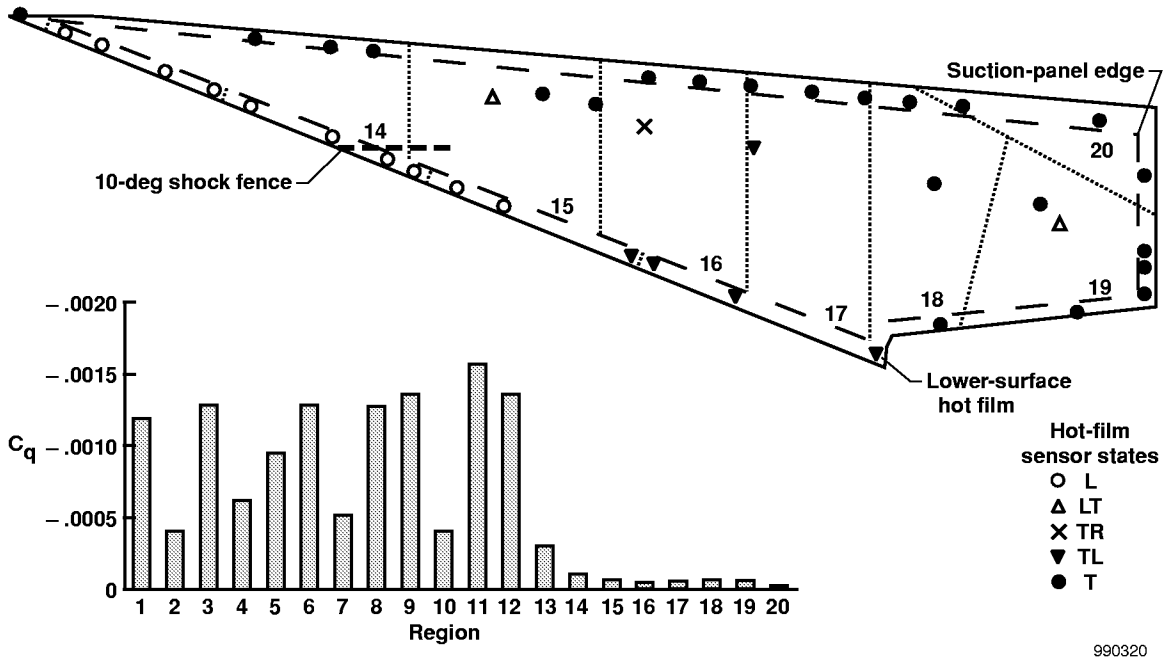

(a) FCV angles: region 11 = 40°; flutes 2 and 3 = 37°; regions 14–19 = 37°.

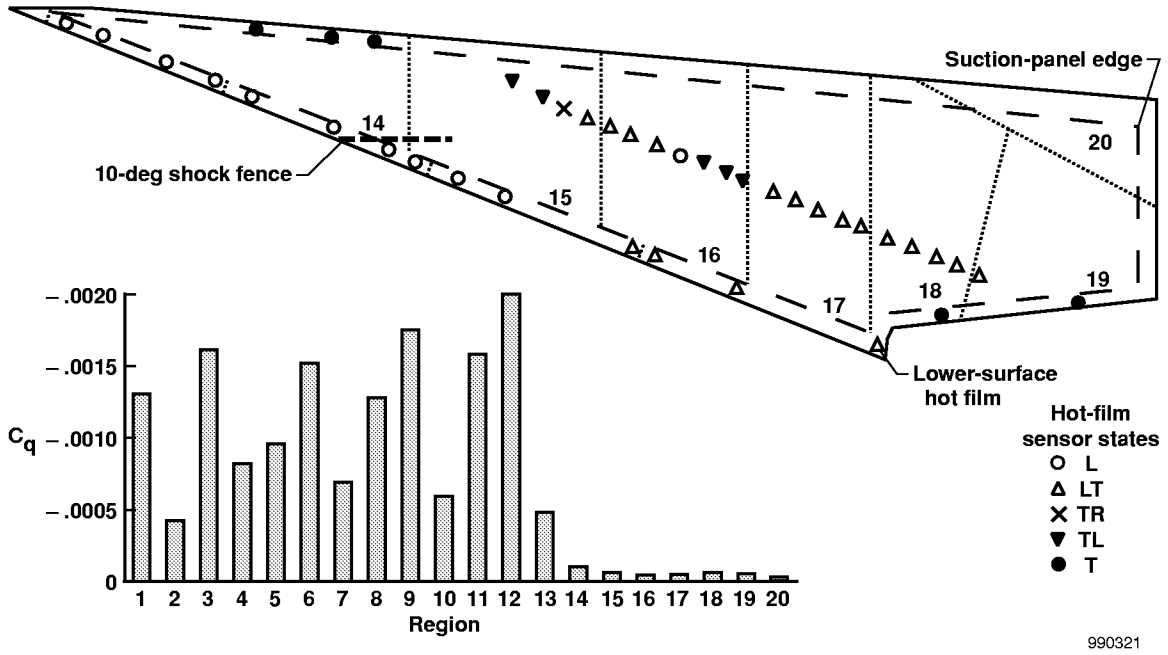

(b) FCV angles: region 11 = 40°; flutes 2 and 3 = 90°; regions 14–19 = 35°.

Figure 22. Suction effects at Mach 2.0, an altitude of 53,200 ft, 3.7° angle of attack, and –1.5° angle of sideslip.

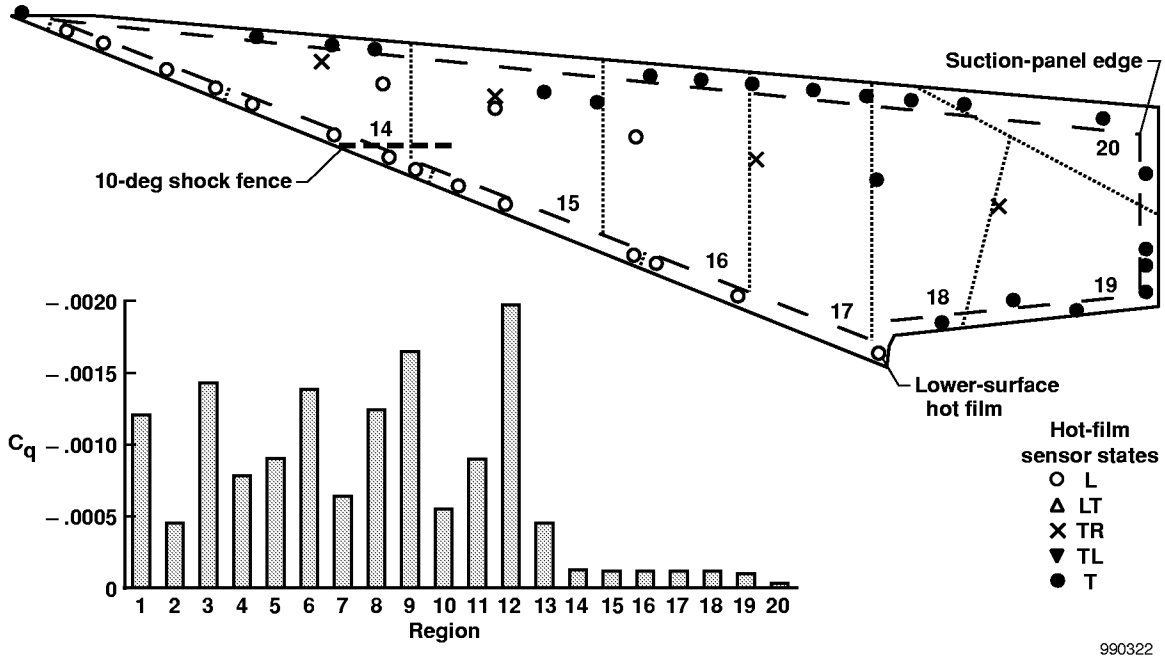

(c) FCV angles: region 11 = 30°; flutes 2 and 3 = 90°; regions 14–19 = 90°.

Figure 22. Concluded.

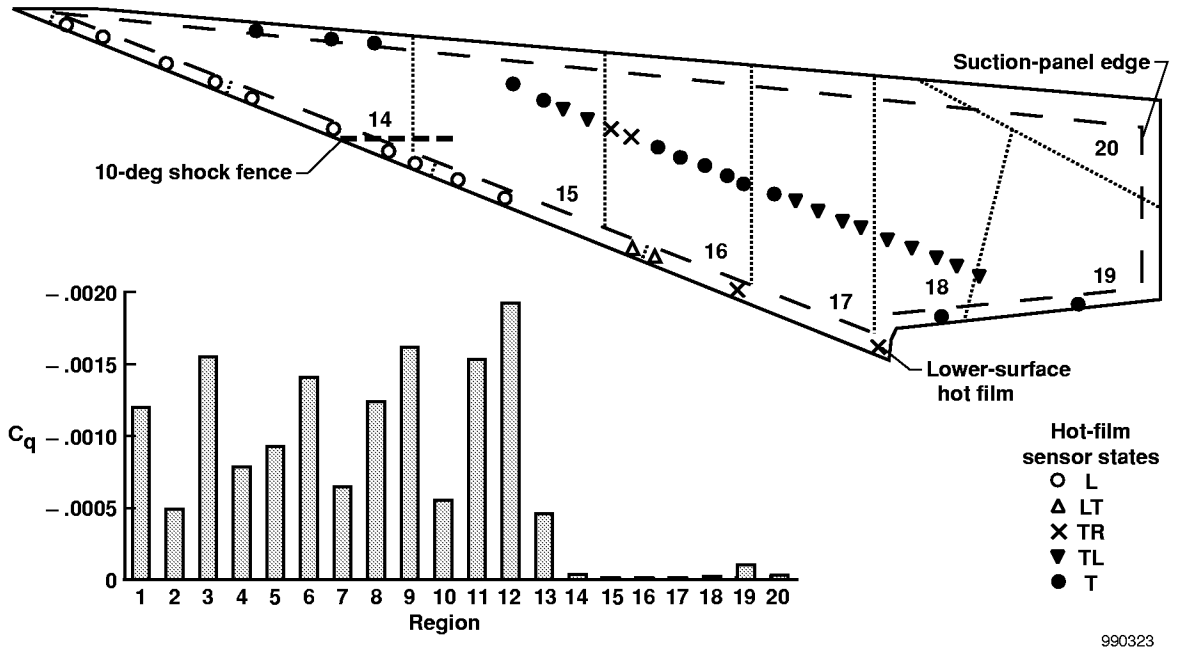

(a) Regions 14–19 FCV angles = 17.5°.

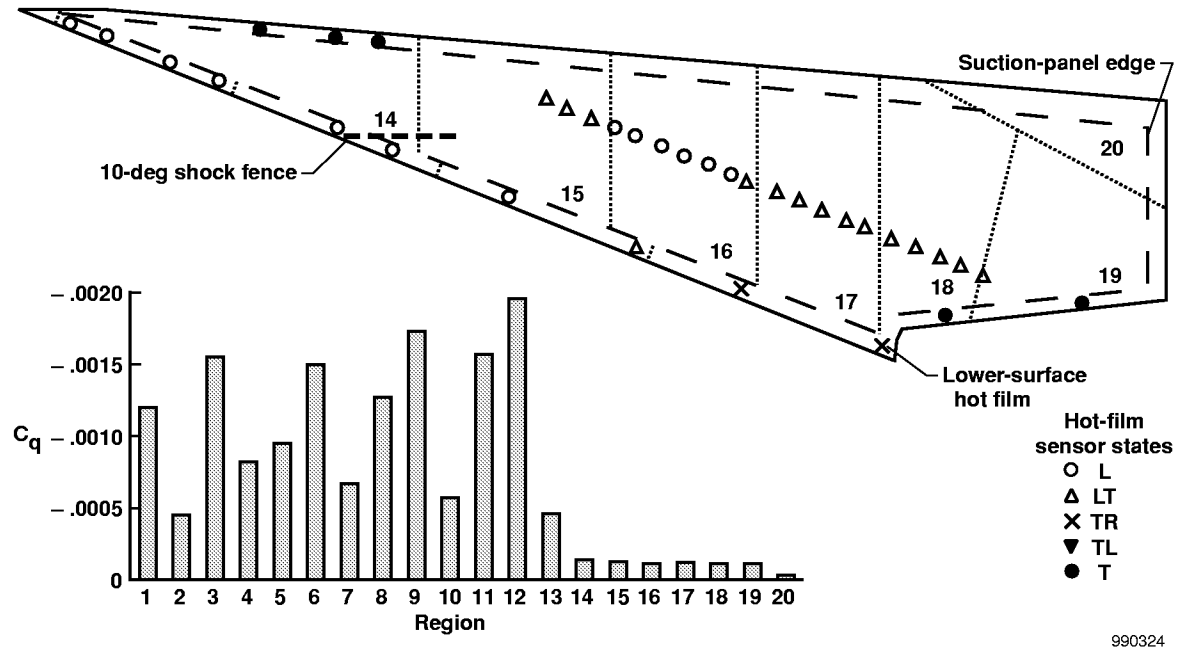

(b) Regions 14–19 FCV angles = 90°.

Figure 23. Rooftop suction effects at Mach 2.0, an altitude of 53,300 ft, 3.7° angle of attack, and –1.4° angle of sideslip.

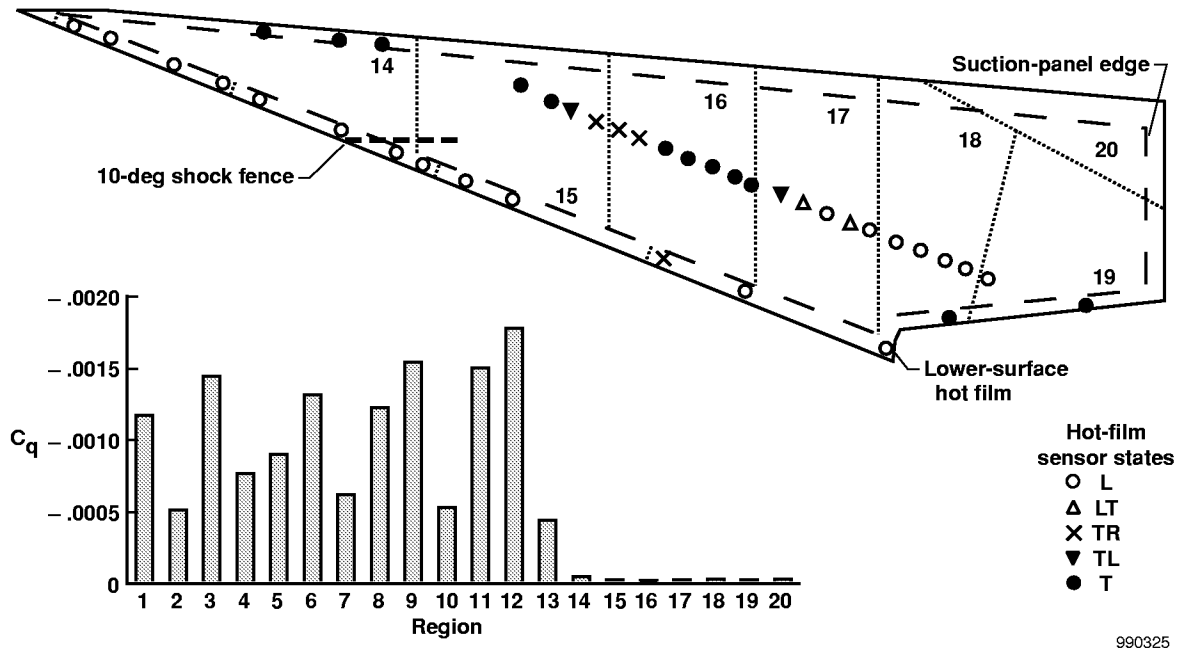

(a) Regions 14–19 FCV angles = 20°.

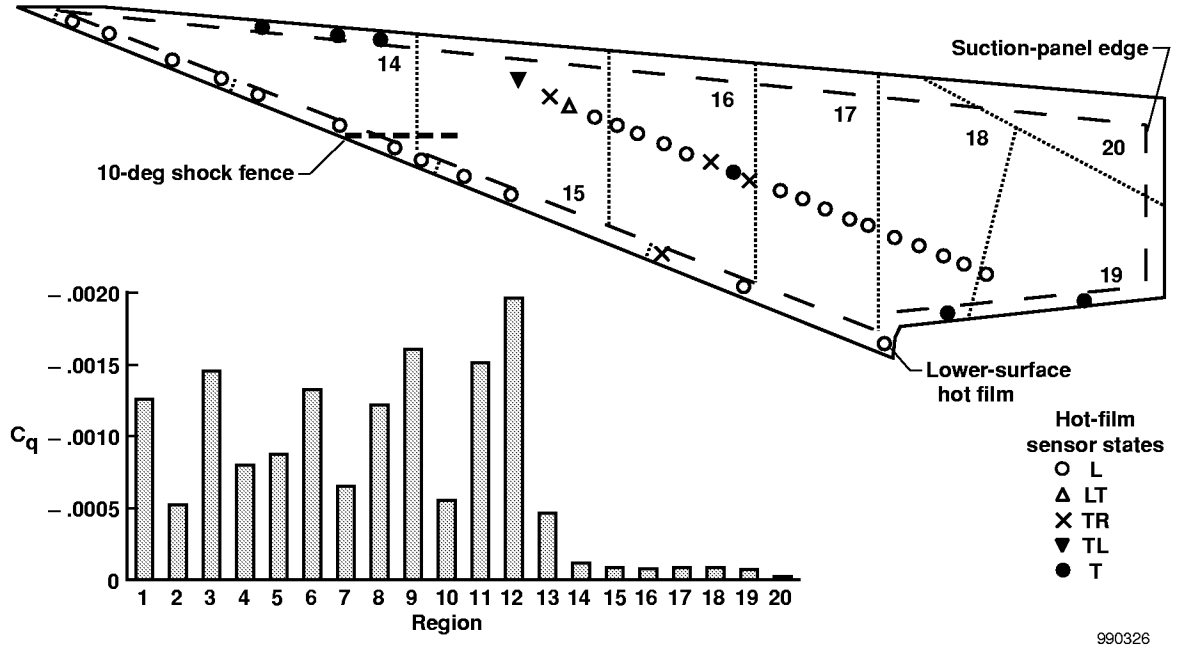

(b) Regions 14–19 FCV angles = 50°.

Figure 24. Rooftop suction effects at Mach 2.0, an altitude of 55,300 ft, 3.7° angle of attack, and –1.4° angle of sideslip.

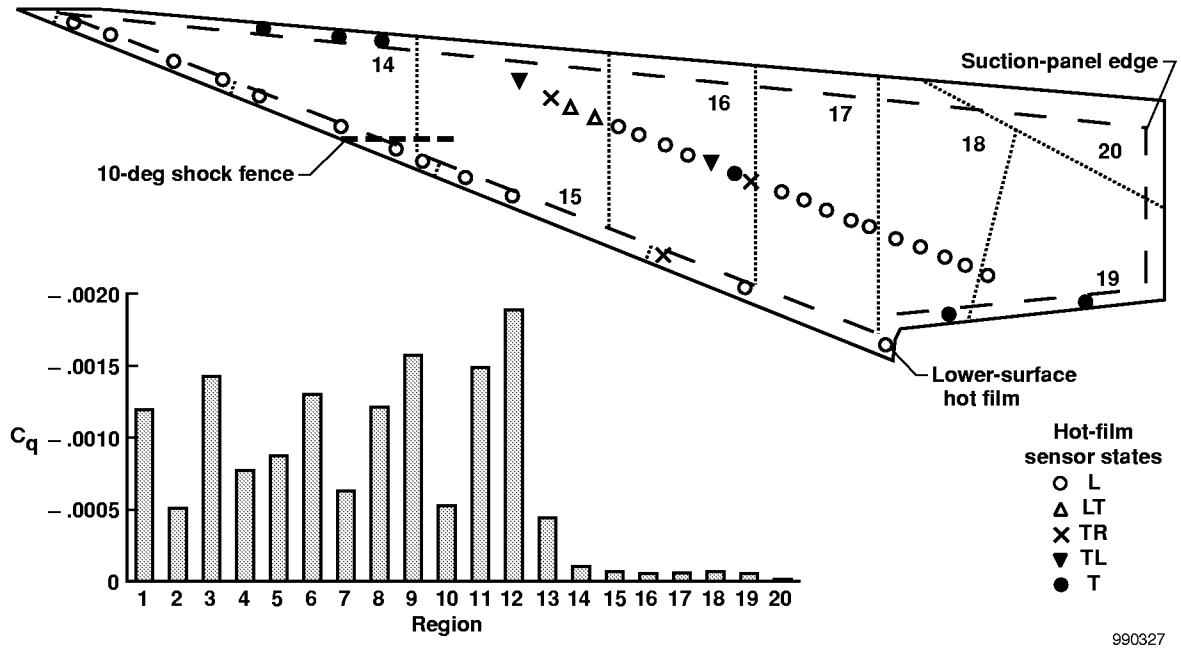

(a) Regions 14–19 FCV angles = 40°.

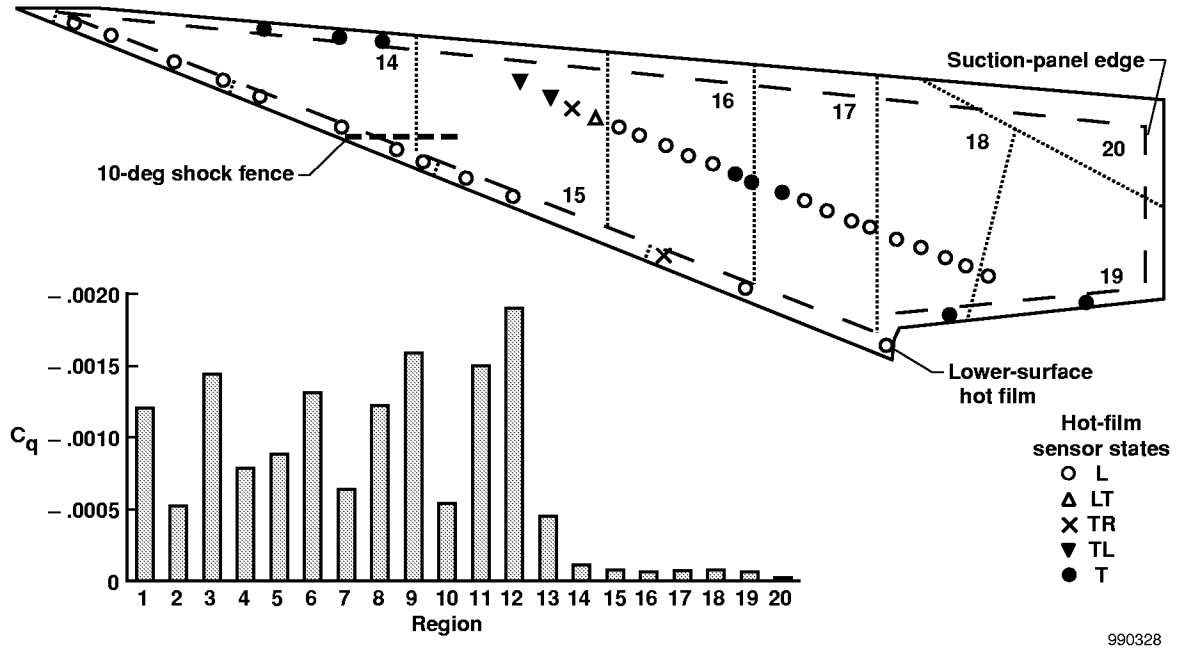

(b) Regions 14–19 FCV angles = 45°.

Figure 25. Rooftop suction effects at Mach 2.0, an altitude of 55,200 ft, 3.7° angle of attack, and –1.4° angle of sideslip.

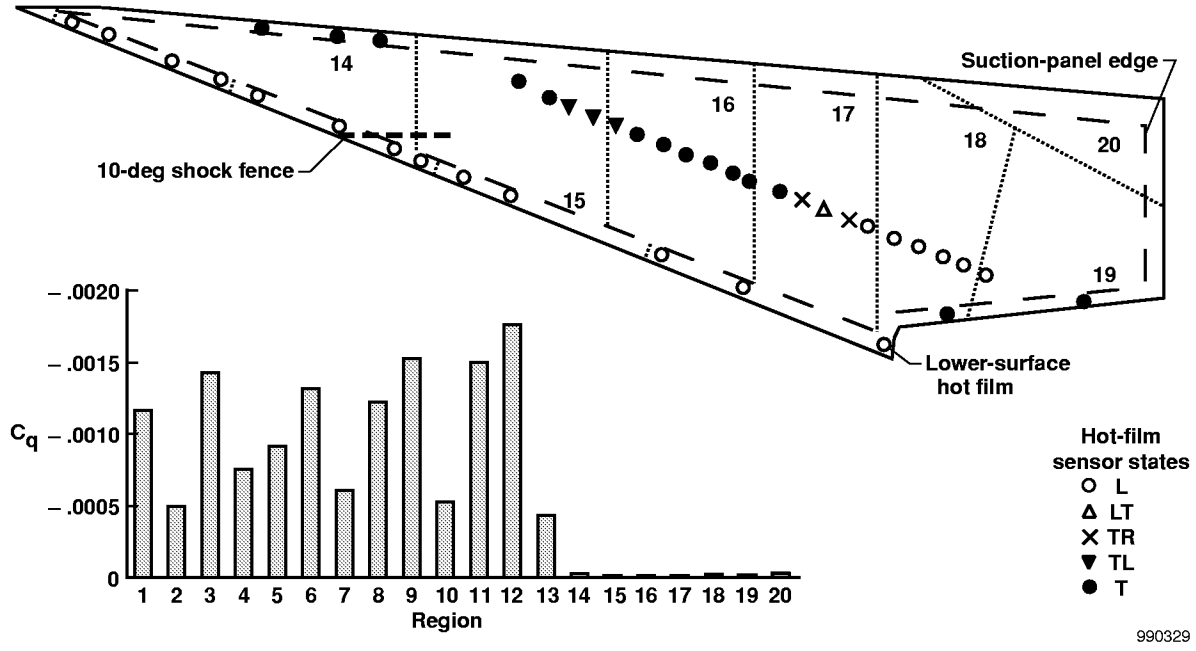

(a) Regions 14–19 FCV angles = 15°.

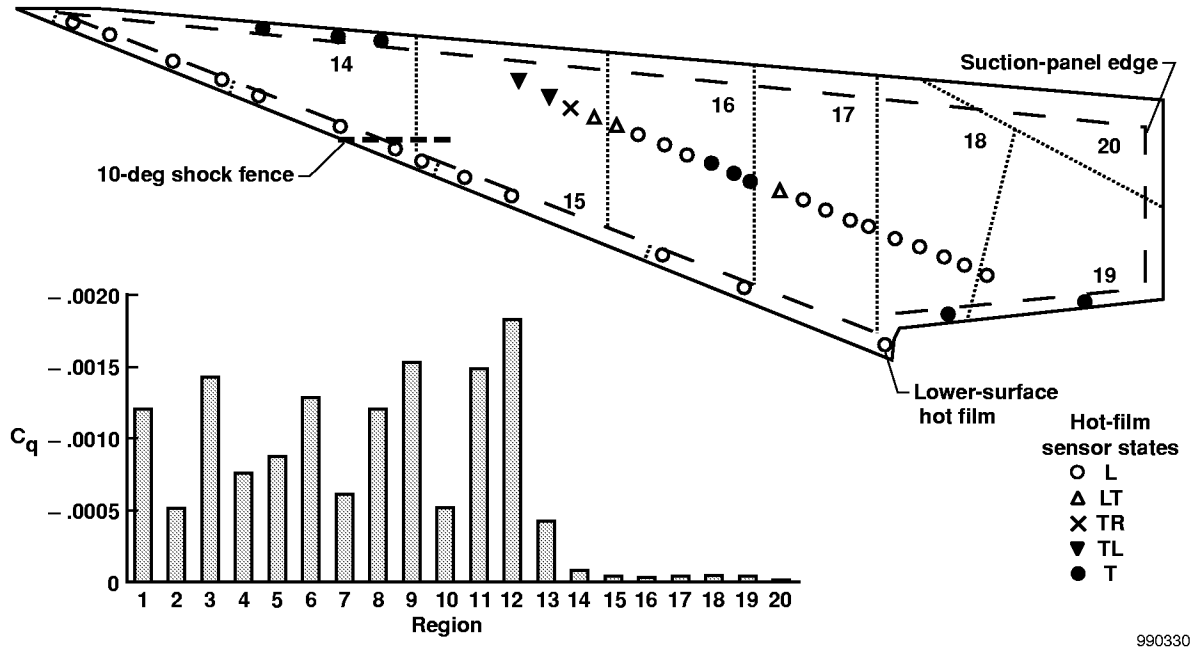

(b) Regions 14–19 FCV angles = 35°.

Figure 26. Rooftop suction effects at Mach 2.0, an altitude of 55,300 ft, 3.7° angle of attack, and –1.4° angle of sideslip.

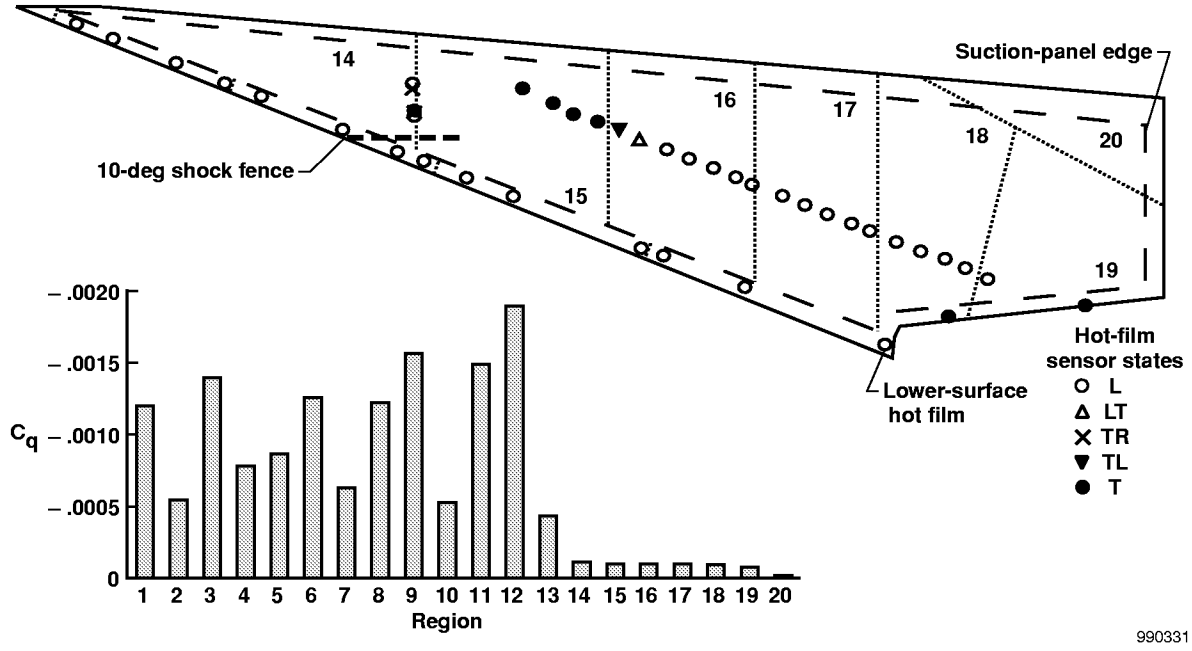

(c) Regions 14–19 FCV angles = 90°.

Figure 26. Concluded.

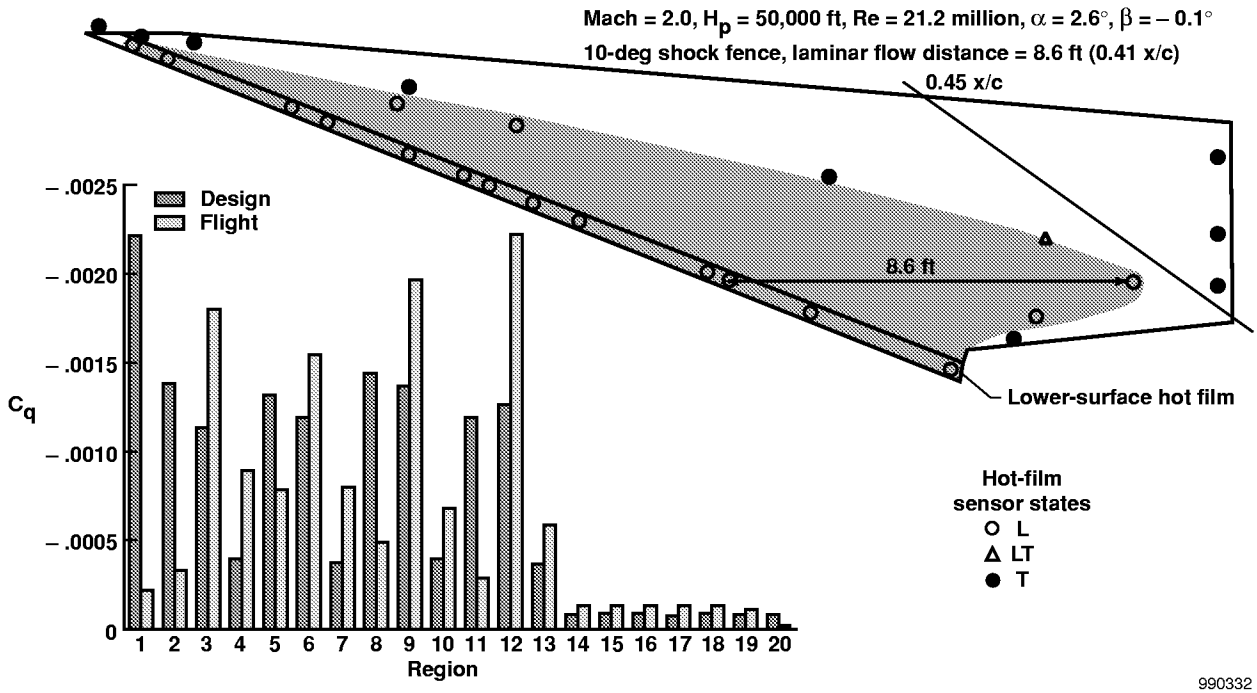

Figure 27. Maximum extent of laminar flow achieved (50,000 ft and 2.6° angle of attack).

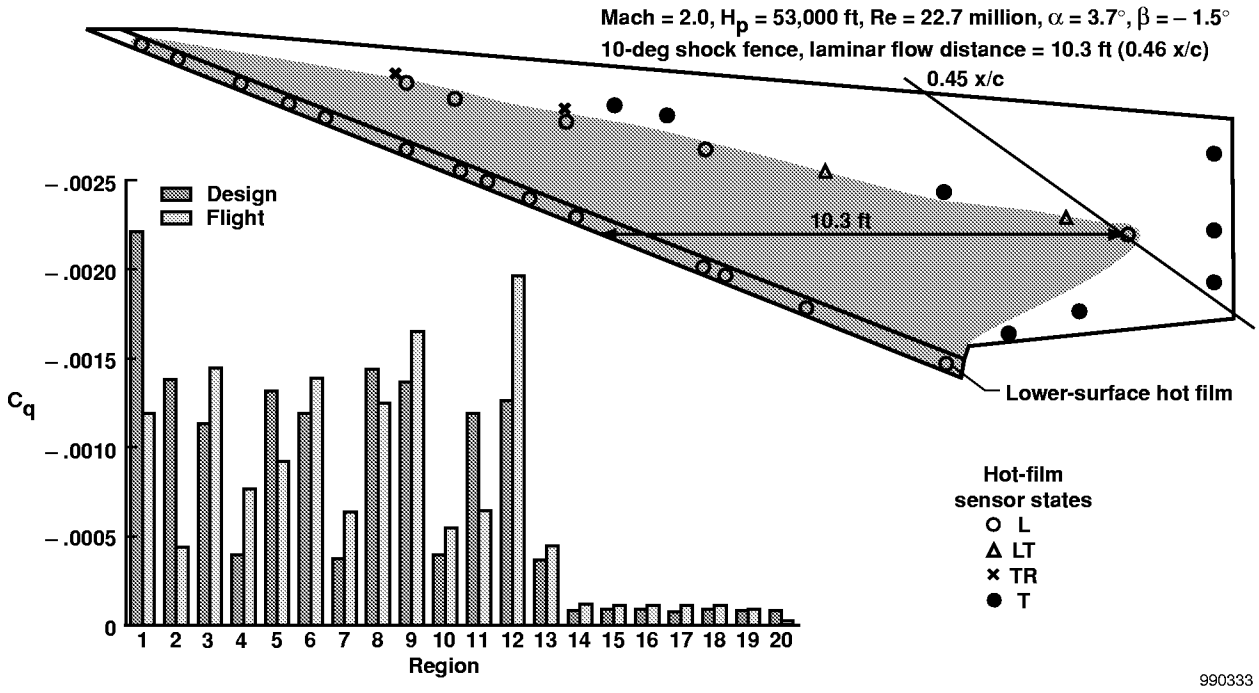

Figure 28. Maximum extent of laminar flow achieved (53,000 ft and 3.7° angle of attack).

APPENDIX

Laminar Flow Control Suction Panel Description

The variable-porosity (hole spacing) suction panel installed on the left wing of the F-16XL-2 airplane was composed of more than twelve million laser-drilled holes of 0.0025-in. constant diameter. The hole spacing, however, equally varied (in rows and columns) from 0.010 to 0.055 in. The titanium panel was divided into 20 regions (fig. 5), each with variable porosity designed to provide within ±5 percent of the design suction level in each region. These regions were further divided into patches that were defined by constant porosity. Table A-1 shows the regions, patches, and hole spacing.

Figures A-1–A-12 show the individual regions, patches, and hole spacing of the suction panel in detail. The numbers within a region represent the patch numbers listed in table A-1. This numbering is consecutive in regions 1–13. In these figures, double lines surround regions and dashed lines surround patches. The aluminum stringers that separated the upper and lower titanium skin are depicted by the rectangles with hatched lines. The large hatched band in regions 15–19 represents the splice joint where two pieces of titanium were joined together to create the suction panel. Suction holes were blocked (that is, no suction existed) wherever hatched lines are shown.

Table A-1. Suction glove hole spacing.

Patch number	Region number	Hole spacing, in.
1	1	0.017
2		0.010
3		0.012
4		0.017
5	2	0.017
6		0.016
7		0.016
8	3	0.016
9		0.016
10		0.016
11	4	0.019
12		0.023
13		0.034
14		0.050
15	2	0.017
16		0.016
17		0.015
18	3	0.015
19		0.014
20		0.014
21	4	0.019
22		0.023
23		0.033
24		0.050
25	5	0.017
26		0.016
27		0.015
28	6	0.017
29		0.017
30		0.017
31	7	0.018
32		0.024
33		0.034
34		0.050
35	5	0.016
36		0.015
37		0.014
38	6	0.015
39		0.015
40		0.015
41	7	0.016
42		0.019
43		0.032
44		0.045
45	8	0.016
46		0.015
47		0.014
48	9	0.014
49		0.014
50		0.014
51	10	0.017
52		0.023
53		0.033
54		0.048
55	8	0.016
56		0.015
57		0.014
58	9	0.014
59		0.014
60		0.014
61	10	0.016
62		0.019
63		0.023
64		0.032
65	11	0.015
66		0.014
67		0.013
68	12	0.013
69		0.012
70		0.012
71	13	0.016
72		0.018
73		0.027
74		0.045
75	11	0.015
76		0.014
77		0.013
78	12	0.013
79		0.012
80		0.012
81	13	0.016
82		0.016
83		0.024
84		0.040
85	14	0.055
86		0.051
87		0.044
88		0.045
89		0.032
90		0.031
91	15	0.035
92		0.031
93	16	0.033
94		0.033
95.1	16	0.031
95.2	17	0.031
96.1	16	0.031
96.2	17	0.031
97.1	16	0.031
97.2	17	0.031
98		0.025
99		0.024
100		0.025
101	18	0.028
102		0.028
103		0.028
104		0.028
105		0.027
106	19	0.030
107	15	0.035
108		0.031
109	16	0.033
110		0.033
111.1		0.031
111.2	17	0.031
112		0.025
113		0.024
114	18	0.028
115		0.028
116		0.027
117		0.027
118		0.027
119	19	0.030
120		0.028
121		0.024
122		0.023
123	20	0.015

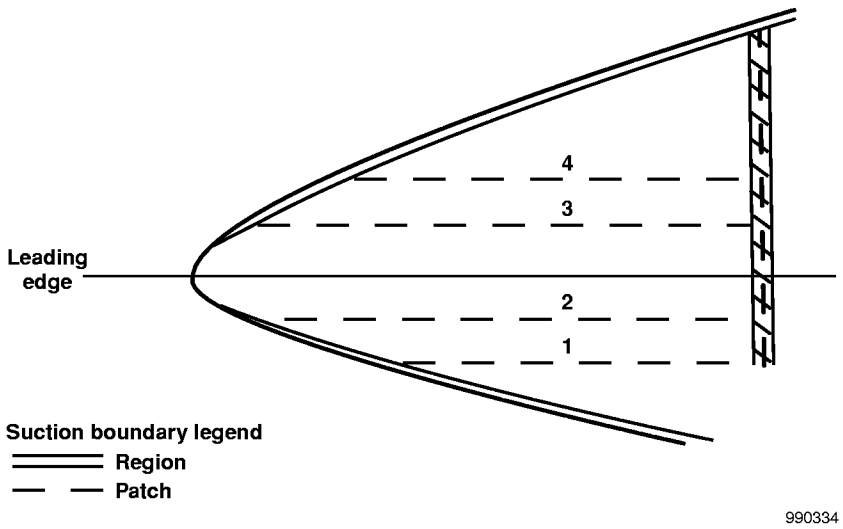

Figure A-1. Suction-panel region 1.

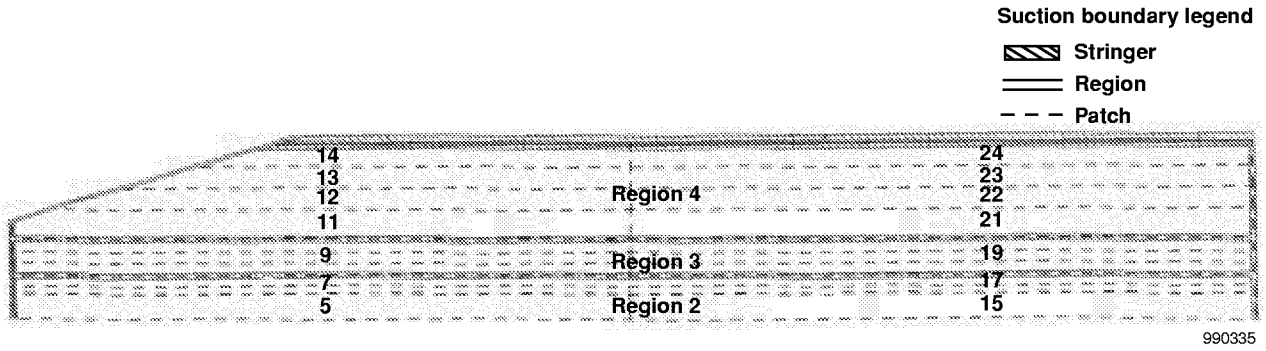

Figure A-2. Suction-panel regions 2–4.

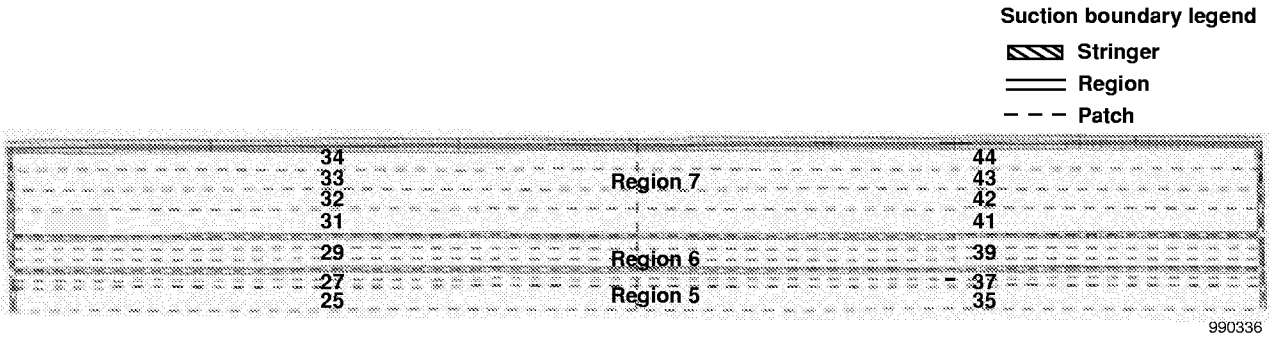

Figure A-3. Suction-panel regions 5–7.

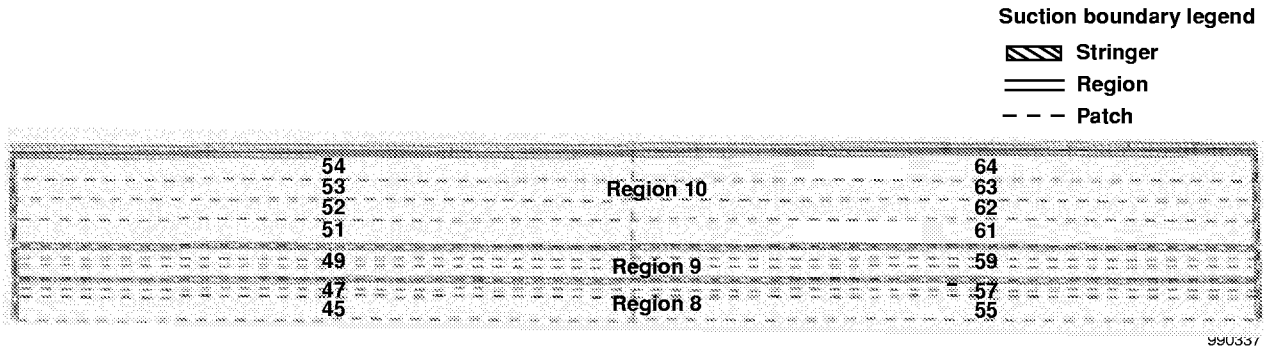

Figure A-4. Suction-panel regions 8–10.

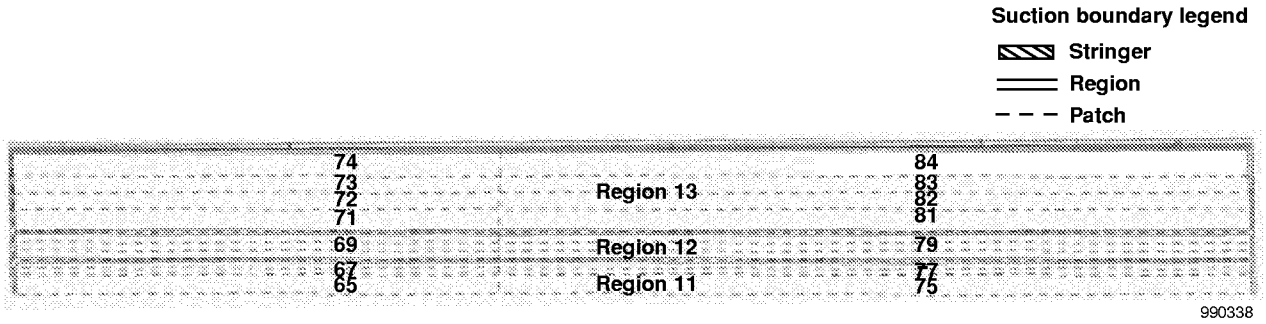

Figure A-5. Suction-panel regions 11–13.

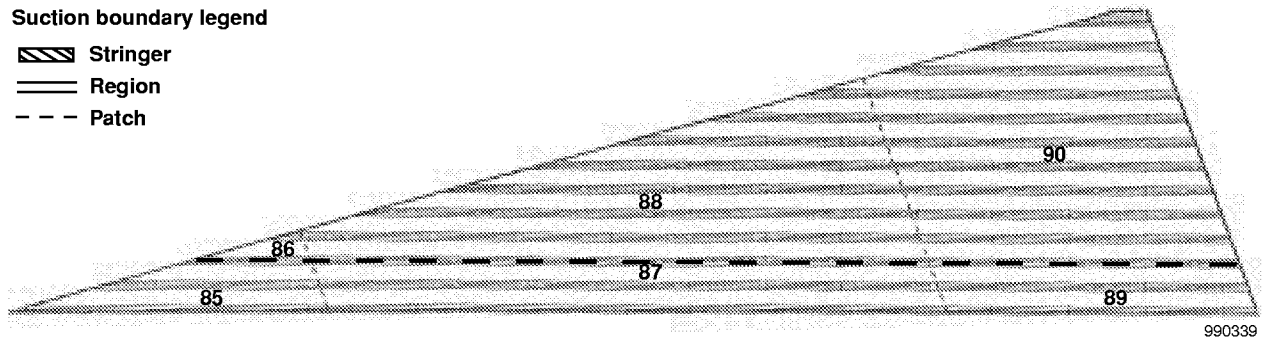

Figure A-6. Suction-panel region 14.

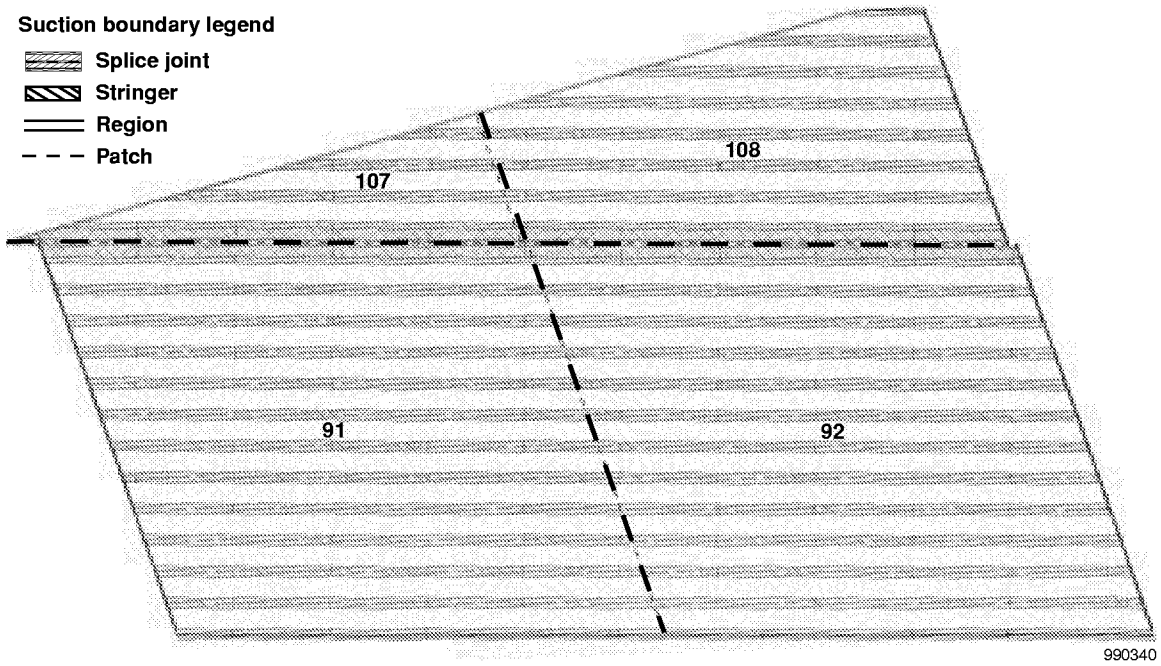

Figure A-7. Suction-panel region 15.

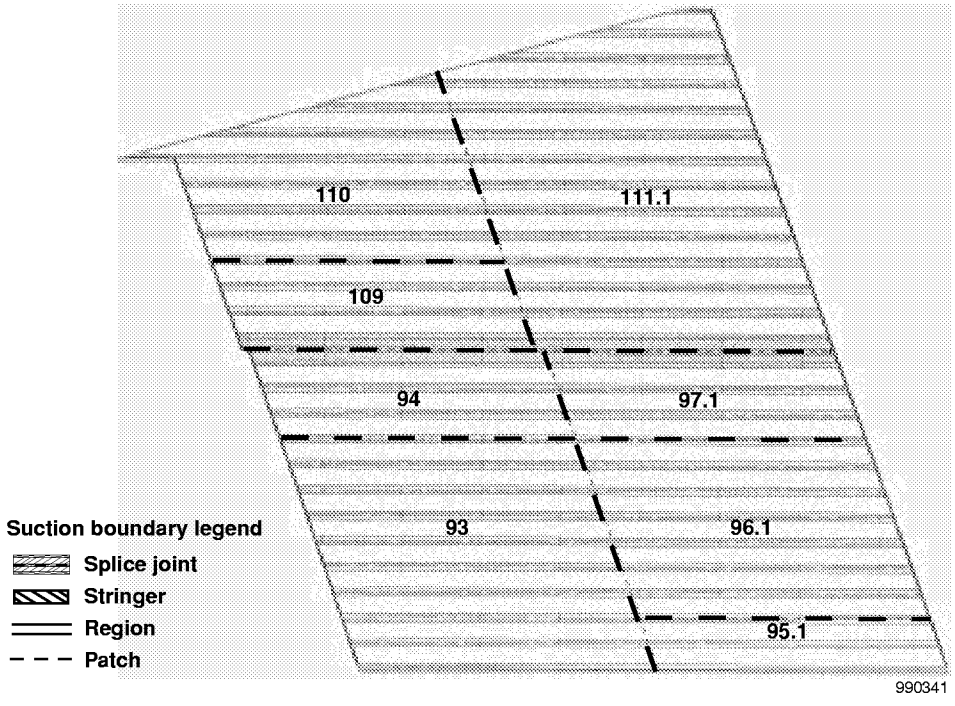

Figure A-8. Suction-panel region 16.

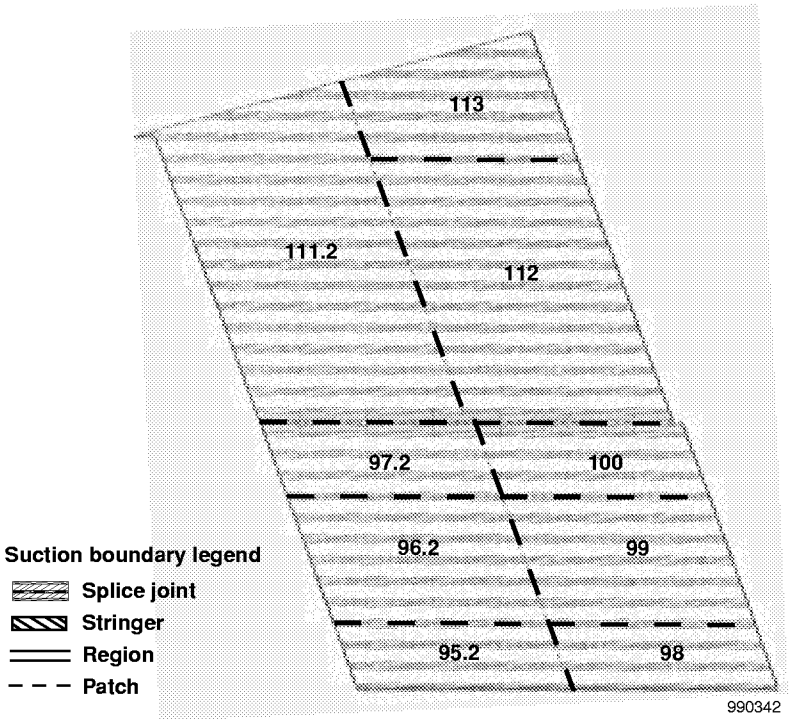

Figure A-9. Suction-panel region 17.

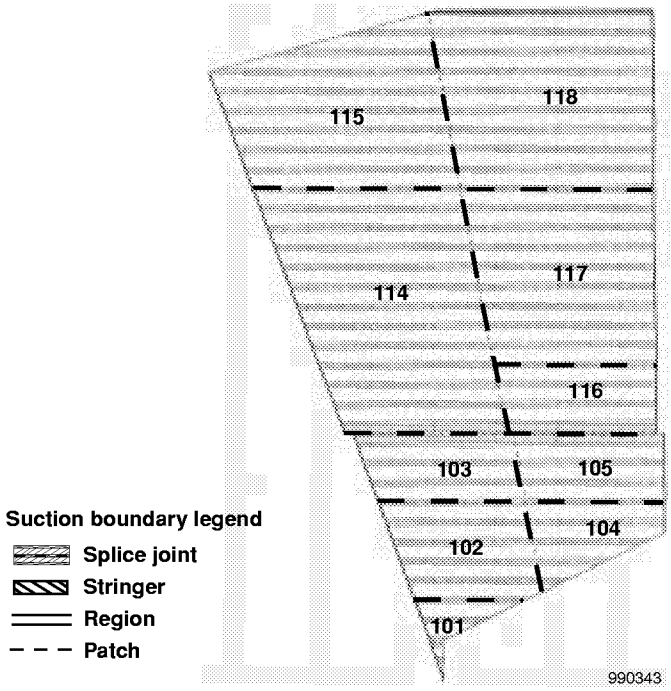

Figure A-10. Suction-panel region 18.

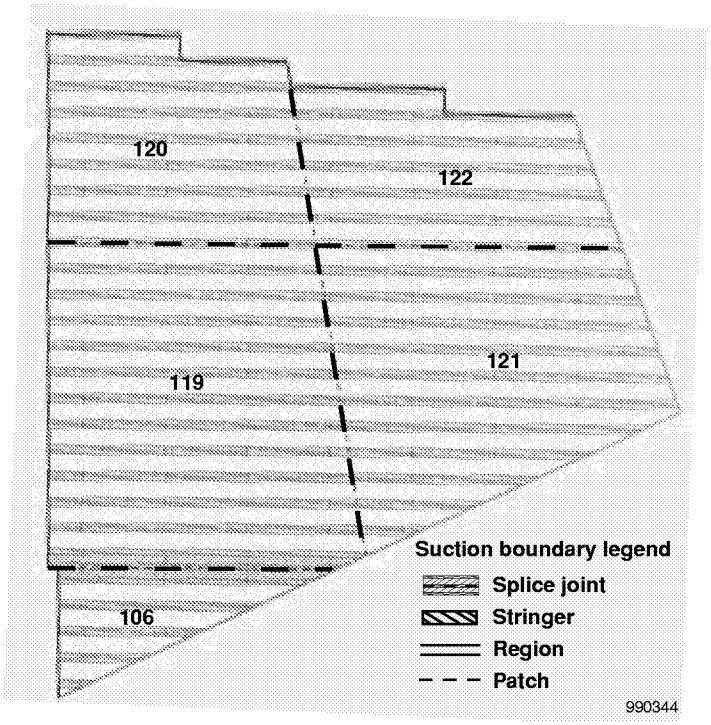

Figure A-11. Suction-panel region 19.

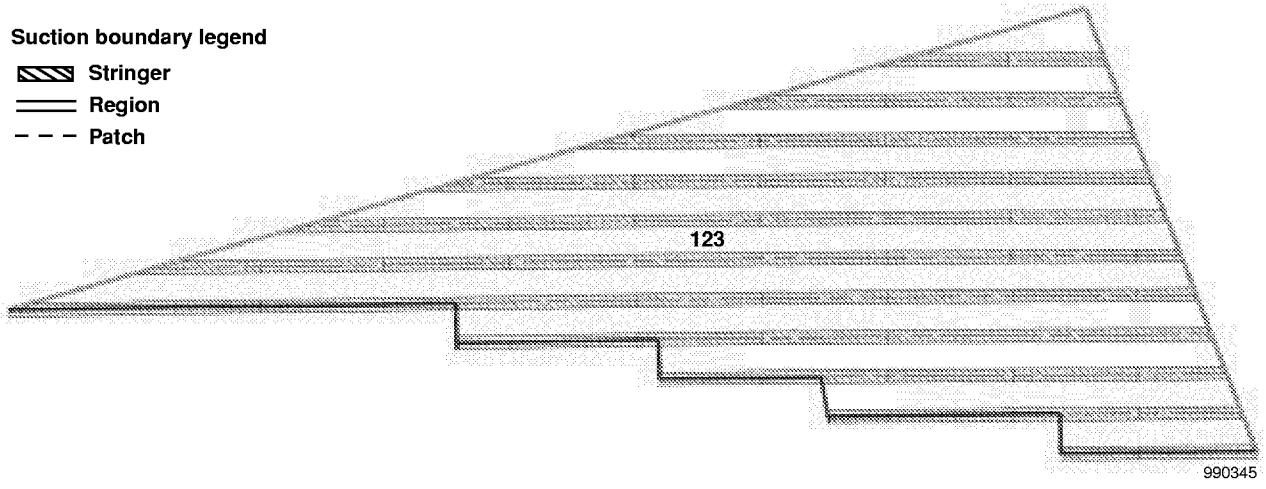

Figure A-12. Suction-panel region 20.

REFERENCES

1. Powell, A. G., S. Agrawal, and T. R. Lacey, *Feasibility and Benefits of Laminar Flow Control on Supersonic Cruise Airplanes*, NASA CR-181817, 1989.

2. Boeing Commercial Airplane Company, *Application of Laminar Flow Control to Supersonic Transport Configurations*, NASA CR-181917, 1990.

3. Pfenninger, Werner and Chandra S. Vemuru, "Design Aspects of Long Range Supersonic LFC Airplanes with Highly Swept Wings," SAE-881397, Oct. 1988.

4. Anderson, Bianca T. and Marta Bohn-Meyer, *Overview of Supersonic Laminar Flow Control Research on the F-16XL Ships 1 and 2*, NASA TM-104257, 1992.

5. Anderson, Bianca T., Bruce H. Rowan, and Stephen F. Landers, *F-16XL Supersonic Laminar Flow Control Glove Initial Flight Test Results*, NASA TM-104270, 1993.

6. Landers, Stephen F., John A. Saltzman, and Lisa J. Bjarke, *F-16XL Wing Pressure Distributions and Shock Fence Results from Mach 1.4 to Mach 2.0*, NASA TM-97-206219, 1997.

7. Anders, Scott G. and Michael C. Fischer, *F-16XL-2 Supersonic Laminar Flow Control Flight Test Experiment*, NASA TP-1999-209683, 1999.

8. Olney, Candida D. and Joseph V. Collura, *A Limited In-Flight Evaluation of the Constant Current Loop Strain Measurement Method*, NASA TM-104331, 1997.

9. Wagner, R. D., D. V. Maddalon, and D. F. Fisher, "Laminar Flow Control Leading Edge Systems in Simulated Airline Service," presented at the 16th Congress of the International Council of the Aeronautical Sciences, Jerusalem, Israel, August 28–September 2, 1988.

10. Chiles, Harry R., *The Design and Use of a Temperature-Compensated Hot-Film Anemometer System for Boundary-Layer Flow Transition Detection on Supersonic Aircraft*, NASA TM-100421, 1988.

11. Anderson, Bianca Trujillo, Robert R. Meyer, Jr., and Harry R. Chiles, *Techniques Used in the F-14 Variable-Sweep Transition Flight Experiment*, NASA TM-100444, 1988.

12. Obara, Clifford J. and Bruce J. Holmes, *Flight-Measured Laminar Boundary-Layer Transition Phenomena Including Stability Theory Analysis*, NASA TP-2417, 1985.

REPORT DOCUMENTATION PAGE

Form Approved
OMB No. 0704-0188

1. AGENCY USE ONLY (Leave blank)	2. REPORT DATE	3. REPORT TYPE AND DATES COVERED
	December 1999	Technical Memorandum

4. TITLE AND SUBTITLE

Boundary-Layer Transition Results From the F-16XL-2 Supersonic Laminar Flow Control Experiment

5. FUNDING NUMBERS

WU 522 31 24 00 24 00 SLF

6. AUTHOR(S)

Laurie A. Marshall

7. PERFORMING ORGANIZATION NAME(S) AND ADDRESS(ES)

NASA Dryden Flight Research Center
P.O. Box 273
Edwards, California 93523-0273

8. PERFORMING ORGANIZATION REPORT NUMBER

H-2382

9. SPONSORING/MONITORING AGENCY NAME(S) AND ADDRESS(ES)

National Aeronautics and Space Administration
Washington, DC 20546-0001

10. SPONSORING/MONITORING AGENCY REPORT NUMBER

NASA/TM-1999-209013

11. SUPPLEMENTARY NOTES

12a. DISTRIBUTION/AVAILABILITY STATEMENT

Unclassified–Unlimited
Subject Category 02
Availability: NASA CASI (301) 621-0390
A pdf file of this report can be found at http://www.dfrc.nasa.gov/DTRS/

12b. DISTRIBUTION CODE

13. ABSTRACT (Maximum 200 words)

A variable-porosity suction glove has been flown on the F-16XL-2 aircraft to demonstrate the feasibility of this technology for the proposed High-Speed Civil Transport (HSCT). Boundary-layer transition data have been obtained on the titanium glove primarily at Mach 2.0 and altitudes of 53,000–55,000 ft. The objectives of this supersonic laminar flow control flight experiment have been to achieve 50- to 60-percent–chord laminar flow on a highly swept wing at supersonic speeds and to provide data to validate codes and suction design. The most successful laminar flow results have not been obtained at the glove design point (Mach 1.9 at an altitude of 50,000 ft). At Mach 2.0 and an altitude of 53,000 ft, which corresponds to a Reynolds number of 22.7×10^6, optimum suction levels have allowed long runs of a minimum of 46-percent–chord laminar flow to be achieved. This paper discusses research variables that directly impact the ability to obtain laminar flow and techniques to correct for these variables.

14. SUBJECT TERMS	15. NUMBER OF PAGES
F-16XL, Hot film, Laminar flow control, Suction, Transition	55
	16. PRICE CODE: A04

17. SECURITY CLASSIFICATION OF REPORT	18. SECURITY CLASSIFICATION OF THIS PAGE	19. SECURITY CLASSIFICATION OF ABSTRACT	20. LIMITATION OF ABSTRACT
Unclassified	Unclassified	Unclassified	Unlimited